Flow (2025), **5** E10
doi:10.1017/flo.2025.6

FLOW CAMBRIDGE UNIVERSITY PRESS

CRITICAL REVIEW

A review on vortex dynamics in the healthy and dilated left ventricles and its application to heart health

Mahesh S. Nagargoje[1,3], Eneko Lazpita[1], Jesús Garicano-Mena[1,2] and Soledad Le Clainche[1,2]

[1]ETSI Aeronáutica y del Espacio - Universidad Politécnica de Madrid, Madrid, Spain
[2]Center for Computational Simulation (CCS), Madrid, Spain
[3]LaBS-CompBiomech, Politecnico di Milano, Milan, Italy
Corresponding author: Soledad Le Clainche; Email: soledad.leclainche@upm.es

Received: 28 August 2024; **Revised:** 29 January 2025; **Accepted:** 21 February 2025

Keywords: Cardiovascular flows; dilated cardiomyopathy (DCM); left ventricle (LV); vortex dynamics

Abstract

Many cardiovascular diseases occur due to an abnormal functioning of the heart. A diseased heart leads to severe complications and in some cases death of an individual. The medical community believes that early diagnosis and treatment of heart diseases can be controlled by referring to numerical simulations of image-based heart models. Computational fluid dynamics (CFD) is a commonly used tool for patient-specific simulations in cardiac flows, and it can be equipped to allow a better understanding of flow patterns. In this paper, we review the progress of CFD tools to understand the flow patterns in healthy and dilated cardiomyopathic (DCM) left ventricles (LVs). The formation of an asymmetric vortex in a healthy LV shows an efficient means of blood transport. The vortex pattern changes before any change in the geometry of LVs is noticeable. This flow change can be used as a marker of DCM progression. We can conclude that the vortex dynamics in LVs can be understood using the widely used vortex index, the vortex formation number (VFN). The VFN coupled with data-driven approaches can be used as an early diagnosis tool and leads to improvement in DCM treatment.

Impact Statement

This manuscript discusses recent advances in the vortex dynamics in the left ventricle and its role in heart disease progression and early diagnosis. The vortex formation index has been formulated in the past and this can be useful for the early diagnosis of flow pattern changes and better treatment management. The change in flow patterns due to structural change in the left ventricle has been critically analysed by discussing hemodynamics in healthy and dilated cardiomyopathy models. Challenges, opportunities and future directions for left ventricle hemodynamics have been discussed.

1. Introduction

Cardiovascular diseases (CVDs) are a leading cause of death globally. According to the World Health Organization (WHO), CVDs account for approximately 31 % of all deaths worldwide. Heart attacks are the major cause of death in CVDs, which account for 25 % of deaths to total deaths. Disabilities due to CVDs can have a significant impact on individuals and communities, and definitely lead to decreased quality of life and increased healthcare costs. Understanding the global burden of heart diseases and their risk factors is crucial for developing effective prevention and treatment strategies.

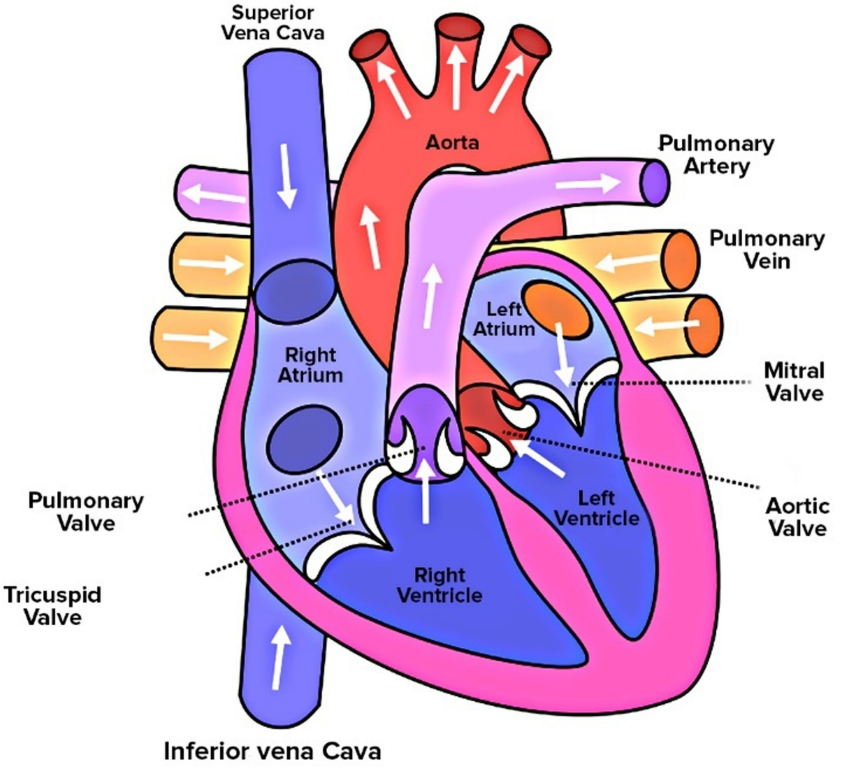

Figure 1. *Schematic of the human heart consisting of four chambers: right atrium, left atrium, right ventricle and LV. Heart valves controlling blood flow between chambers are shown in the whole heart model. Schematic is reused under GNU free documentation licence from the Free Software Foundation (Human Heart, 2023).*

The human heart consists of four chambers, a pair of atriums and ventricles, as shown in Figure 1. Atria are used for collecting blood whereas ventricles are used for pumping blood. The right atrium collects the deoxygenated blood from various organs and the left atrium collects oxygenated blood from the lungs via pulmonary veins. The right ventricle pumps the blood to the lungs for oxygenation and the left pumps the oxygenated blood to the rest of the body. The left ventricle (LV) plays a crucial role in the functioning of the heart, being responsible for supplying blood to all the tissues throughout the body. The LV collects the oxygenated blood from the left atrium during diastolic filling and ejects the blood during systole. The vortex patterns during diastolic filling differentiate between normal and abnormal LV flow dynamics. Asymmetric and smooth vortex formation in the LV is considered a healthy means of blood transport. However, the presence of an unnatural vortex in the LV is often associated with cardiac diseases. One of the very common LV diseases is dilated cardiomyopathy (DCM), which is a condition in which the LV chamber becomes enlarged, with thinner and weaker walls, which corresponds to decreased cardiac function (Grossman et al., 1974; Jefferies and Towbin, 2010). Due to changes in the anatomy of the LV, the flow and vortex patterns change. It has been observed that DCM patients have less ordered blood flow patterns with decreased vortex strength, a decrease in flow propagation velocity and more stagnation at the apex of LV (Baccani et al., 2002b; Loerakker et al., 2008). Changes in blood flow patterns have been analysed using computational fluid dynamics (CFD), by investigating various flow and vortex indices.

Vortex patterns in the LV are crucial for efficient blood transport and have been studied extensively in CVD. Past studies have shown that abnormal flow patterns due to vortex breakdowns can lead to

https://doi.org/10.1017/flo.2025.6 Published online by Cambridge University Press

energy dissipation and increased stagnation zones (Pedrizzetti et al., 2014). An increase in stagnation zones leads to clot formation and a decrease in ejection fraction increases the in-turn risk for heart failure (Pedrizzetti and Domenichini, 2005, 2015; Pedrizzetti and Sengupta, 2015). The vortex in a healthy LV is asymmetric and non-planar, which avoids eddy formation by recirculating and propagating them towards the outlet without colliding with each other. The asymmetric doughnut-shaped vortex ring formation occurs during diastolic filling at the end of the E-wave and A-wave (M Elbaz et al., 2014; Töger et al., 2012). An index has been formulated to characterise the vortex ring formation quantitatively and its propagation: the vortex formation number (VFN). The VFN measures the length-to-diameter ratio of the ejected fluid, which is directly proportional to ejection velocity and inversely proportional to orifice opening. A VFN between 3 and 5 has been considered optimal, whereas values beyond 5 lead to instability and excessive energy dissipation (Gharib et al., 2006). Recently, the vortex in the LV has been used as an early predictor of cardiovascular outcomes. It is believed that abnormal flow patterns in the LV could signal the presence of heart malfunction even before noticeable structural changes are evident (Pedrizzetti et al., 2014). In contrast, utilisation of the VFN as a marker for cardiac function has been argued experimentally and it has been proposed that the VFN is not an index of cardiac function and it should not be used as an index (Pasipoularides et al., 2015; Stewart et al., 2012). However, few clinical studies have shown the use of the vortex formation time as an indicator of cardiac function, but they have pointed out the discrepancies in heart failure with preserved ejection fraction and sphericity of the LV (Martínez-Legazpi et al., 2014; Poh et al., 2012).

Numerical studies have become an essential tool in understanding the hemodynamics and vortex patterns of the LV over the last couple of decades. Computational fluid dynamics has been used to study the blood flow patterns in the LV, providing insights into the vortex dynamics in both healthy and diseased hearts (Chan et al., 2013b; Doost et al., 2016a). The CFD studies were started with two-dimensional models of the LV and analysed the formation of the vortex in a healthy and a diseased LV and found that the flow wave propagation velocity reduced in a dilated LV (2002b, Baccani et al., 2002a; Chan et al., 2013c; Loerakker et al., 2008; Pierrakos and Vlachos, 2006; Vierendeels et al., 2000). Further, numerical simulation of three-dimensional ideal healthy LV models found asymmetric vortex generation (Schenkel et al., 2009). Recently, high-resolution imaging techniques such as MRI have been combined with CFD to obtain detailed flow characteristics and improve our understanding of the complex hemodynamics in the LV (Khalafvand et al., 2015; Labbio and Kadem 2018). Past studies investigated that the effect of inlet waveform specified at pulmonary veins does not affect flow patterns in patient-specific LV and stagnation zones at the apex of the LV are prone to thrombi formation (Lantz et al., 2019; Liao et al., 2016). Most of the studies have the major limitation of considering the walls of the LV as rigid, which is not close to the *in vivo* situation. Realistic studies have modelled the contraction and expansion of the LV using a moving mesh approach. Consideration of moving walls improves the accuracy of the vortex pattern prediction and the hemodynamics in the LV (Chan et al., 2013a, 2019; Cheng et al., 2005; Vedula et al., 2014). Recently published articles considered the coupling of mitral valve (MV) movement with LV hemodynamics and found that it helps in risk stratification and optimisation of heart therapies (Gao et al., 2017).

Despite the complexity of cardiac flows, this review will focus on showing an extensive review of the formation of the vortex. It should be acknowledged that factors such as mitral and aortic valve modelling, patient conditions and disease alterations influence the flow. However, we will specifically examine the literature on the vortical patterns in these flows, setting aside other phenomena beyond the scope of this paper.

This review, which includes over 125 references, summarises significant advances from the last two decades in the fundamentals of cardiac flows from a numerical perspective. It also compares these with experimental or medical data. The selected publications provide a comprehensive overview of the current technology for studying cardiac flows, offering new insights into the flow physics of healthy and diseased hearts. Additionally, this review highlights the need for validating optimal and abnormal vortex patterns using extensive datasets of experimental data and clinical observations. The review also considers the potential of data-driven methods, including machine learning, for identifying abnormal vortex

https://doi.org/10.1017/flo.2025.6 Published online by Cambridge University Press

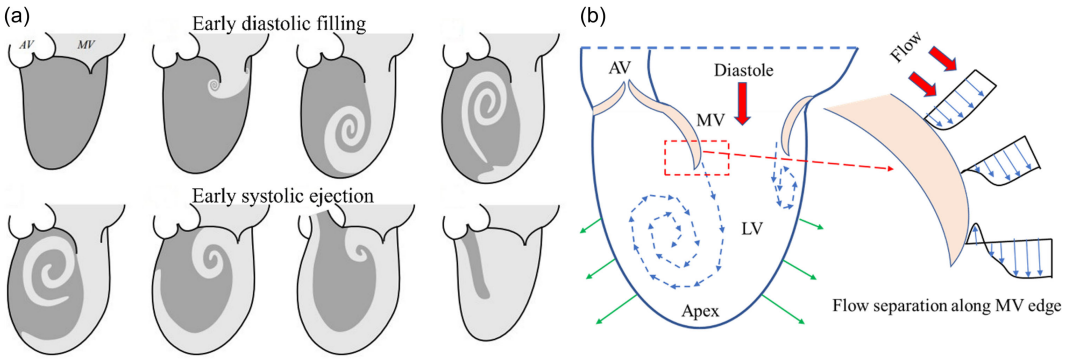

Figure 2. *(a) Schematic of blood transport during filling and ejection of blood through a healthy LV, dark grey: old blood, and light grey: new blood. Adapted with permission from a previous numerical study (Di Labbio et al., 2022). (b) Blood flows (thick red arrow) into the LV through the MV. At the trailing edge of the MV, blood develops two shear layers of different velocities. The boundary layer separation leads to an adverse pressure gradient and the blood stream rolls up into a vortex.*

patterns as markers for heart function monitoring. Trained machine learning models could become invaluable for assessing early outcomes of heart valve surgeries and indicating the success of various heart procedures. This opens new discussions on the condition selection necessary for accurate CFD simulations of the LV.

2. Vortex dynamics in the left ventricle

The filling of blood in the LV occurs due to the MV opening and the flowing of blood into the LV through the small MV orifice. The MV consists of two triangular cusps of unequal size; they are stronger in mechanical strength than tricuspid valves. The expansion of the LV during early diastolic flow (during the E-wave) creates a reduced pressure in the LV, which generates a gradient for blood flow from mitral leaflets (high pressure) to the LV apex (low pressure). Decreased pressure thus generated in the LV chamber induces the mitral cusps to open. Blood filling from the left atrium is observed while low pressure exists in the LV. Atrium contraction also contributes to LV filling, which is called A-wave filling. The blood flow through a healthy MV is generally laminar: this promotes a normal asymmetric vortex formation in the LV, as shown in Figure 2(a). The smooth transfer of blood is observed during the systolic phase in a healthy heart.

The boundary layer separation of the MV leaflet's trailing edge and the subsequent development of shear layers is the triggering point of vortex formation. During blood flow through the MV, blood develops shear layers of increasing velocity away from the valve edge, as shown in Figure 2(b). The velocity of the blood layer close to the valve edge is almost zero and away from the valve edge shows a higher velocity. Due to the curvature of the MV edges, flow separation occurs, and due to the gradient in velocity shear layers, the bending of the streamlines induces a rolling motion of the blood, and the subsequent formation of a vortex on both sides of the MV. During the roll-up process, the distance between adjacent vortex turns reduces and the vortex cone forms a conical-like flow trajectory. The base of a cone can be referred to as the initial vortex size, whereas the tapered end of the cone is considered as the end of the vortex helical path. The vortex formation in the LV is a smoother (in contrast to chaotic or turbulent flow) phenomenon due to a confined and limited expansion of the LV, which restricts the vortex size from growing. The formation of a vortex stores the incoming translational kinetic energy into a rotary motion. Ill-functioning LVs show abnormal vortex formation flows and these may lead to turbulence and excessive energy dissipation. It has been reported that malfunctioning of the heart typically results in changes in the vortex dynamics or the size and number of vortices.

https://doi.org/10.1017/flo.2025.6 Published online by Cambridge University Press

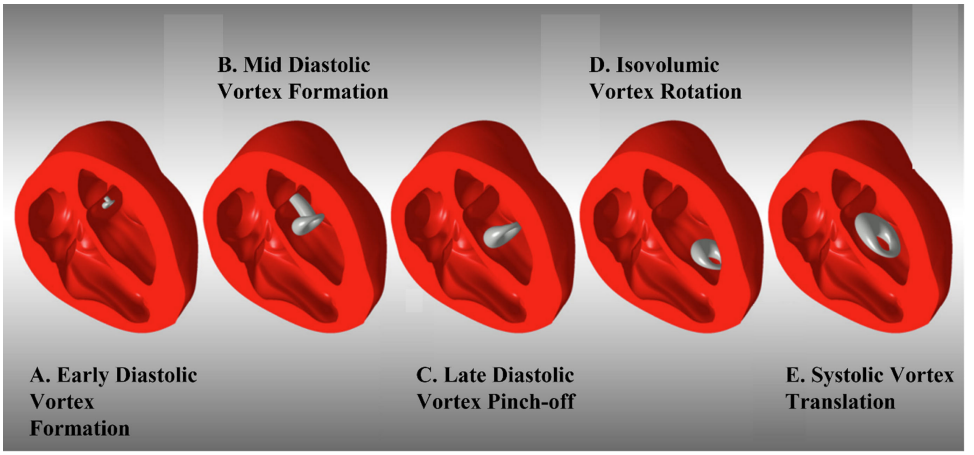

Figure 3. *Vortex formation in the healthy LV and the vortex ring pinch-off and rotation during a cardiac cycle. Adapted with permission from a previously published article (Kheradvar et al., 2012).*

The vortex formed in a healthy LV is asymmetric: these asymmetries have been proven beneficial for the smooth transfer of blood from the MV toward the LV base. The formed vortex decays at the end of the diastole and a difference in decay rate was observed for normal and abnormal filling (Brindise et al., 2020). This asymmetric shape is due to the unbalanced shape of the MV, since the anterior leaflet (Figure 2b left cusp of the MV) is larger than the posterior leaflet (right cusp of the MV). Also, the area available for flow and fluid wall interaction is different for the leaflets. The posterior leaflet has a free edge and more area to flow while the anterior leaflet finds the LV wall adjacent to the MV leaflet. The generated primary and secondary vortex rings at the MV propagate into the LV until they get pinched off from the flowing jet at the end of the E-wave (primary vortex ring) and A-wave (secondary vortex ring) during the diastolic phase. The vortex can be visualised as the doughnut-shaped ring in Figure 3. The asymmetry in the vortex size is also reflected in the vortex ring thickness. The ring thickness is lower on the posterior side than on the anterior. The ring thickness depends on leaflet lengths and non-homogeneous pressure gradient in the LV. The vortex ring rotates while propagating towards the LV apex. Moreover, the ring-shaped vortex changes its axis of rotation by ninety degrees and efficiently aligns itself in the flow direction towards the aorta. A lower thickness ring shifts towards the LV apex by rotation and can be an efficient means of momentum transfer, as shown in Figure 3 (Kheradvar et al., 2012).

Figure 4(a–e) shows the intraventricular pressure distribution during LV filling in a healthy subject. Before the E-wave peak, the pressure gradient points from the MV orifice towards the apex and the flow is driven in the same direction. The generation of a lower pressure zone at the apex is the result due to LV expansion. After the peak velocity has been attained, the pressure distribution reverses until the apical pressure exceeds that of the base. This pressure gradient directs the flow towards the middle cavity of the LV. During diastasis, the pressure gradient does not significantly vary in the LV cavity. Again, the pressure gradient from base to apex is generated due to the contraction of the atrial chamber before the A-wave peak. Finally, the contraction of the LV results in a pressure gradient from the apex to the LV outlet, and blood smoothly transfers towards the aorta in the form of stable, orderly converging vortices. Similarly, figure 4(f–i) shows the velocity streamlines and vortex ring formation during peak E-wave and A-wave. The formation of primary and secondary vortex rings is clearly seen during the E and A waves, respectively.

Recall that LV dysfunction and abnormal vortex patterns are strongly connected. The difference between efficient and inefficient LV ejection can be understood and even quantified more easily by

https://doi.org/10.1017/flo.2025.6 Published online by Cambridge University Press

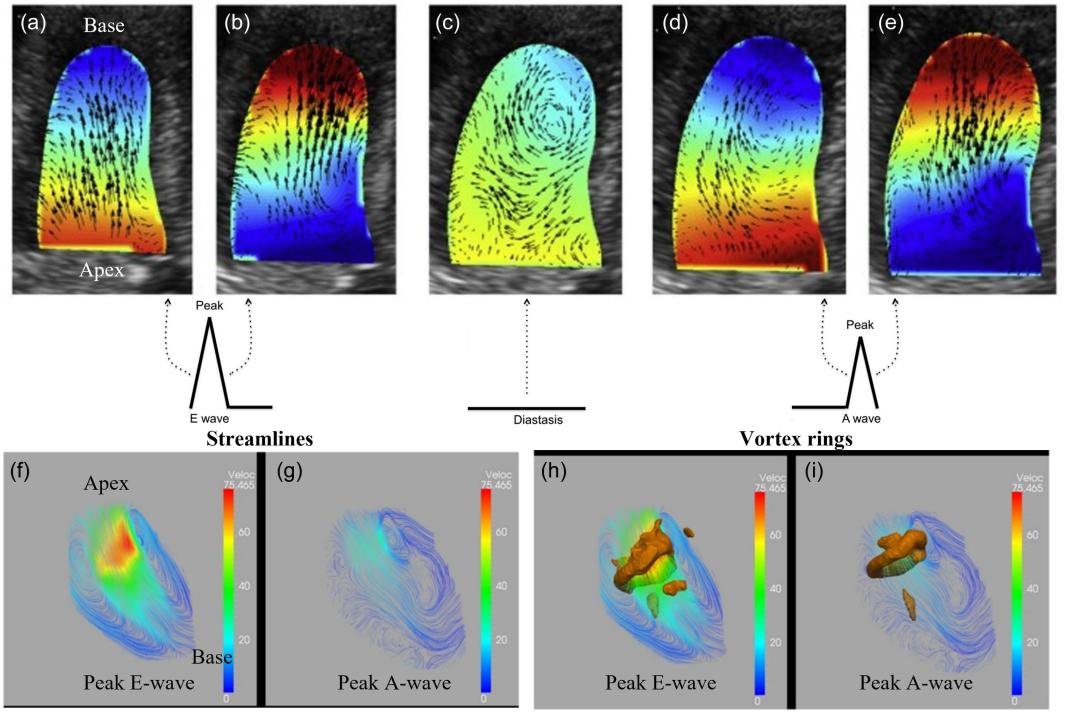

Figure 4. *Intraventricular pressure distribution in the LV during the diastolic filling phase in a healthy subject. (a) Pressure gradient increases from base to apex and flow accelerates accordingly during early diastole before E-wave peak; (b) pressure gradient is directed from apex to base and inflow decelerates during end of E-wave; (c) no significant pressure gradient occurs during diastasis; (d) pressure gradient increases from base to apex and flow accelerates accordingly during beginning of atrial systole before A-wave peak; (e) pressure gradient is directed from apex to base and accelerating flow towards LV outlet by smooth vortex rotation. Blue: lower, and red: higher values. Streamlines at (f) peak E-wave, (g) peak A-wave, vortex rings (lambda 2 criteria) at (h) peak E-wave, (i) peak A-wave. Adapted with permission from a previously published article (M Elbaz et al., 2014; Mele et al., 2018).*

introducing several vortex formation indices. The VFN defines the optimal range of blood transport, between 3.5 and 5.5. It can be expressed as given in equation 1

$$VFN = \frac{\overline{U}}{\overline{D}}.T, \tag{1}$$

where $\overline{U}$ is the time-average velocity of the bloodstream coming out from MV, $\overline{D}$ is the time-average mitral orifice diameter and T is the duration of the diastolic filling during the E-wave.

The VFN range between 3.5 and 5.5 has been observed as an efficient means of fluid transport. Indeed, all biological propulsions observed in nature are shown a VFN between 3.5 and 5.5 (Dabiri, 2009). If the range goes beyond 5.5 the vortices are formed as a trailing jet, which is inefficient (Gharib et al., 1998). The fluid transport by vortices is more efficient than by a steady jet or trailing jet (Krueger and Gharib, 2003; Xiang et al., 2018). The vortex ring will continue to grow until VFN reaches 4. For VFNs greater than 4, vortex instability results, which in turn prevents vortex growth on the grounds of energetic constraints: this leads to the trailing jet regime (Dabiri and Gharib, 2004; Gharib et al., 1998). A single vortex ring is formed when the VFN is less than or within the optimal range. For example, mitral stenosis reduces the area available to flow and increases the bloodstream velocity, which leads to an increase in the VFN beyond the optimal range. In contrast, a dilated LV decreases the VFN to below 3.5, leading

https://doi.org/10.1017/flo.2025.6 Published online by Cambridge University Press

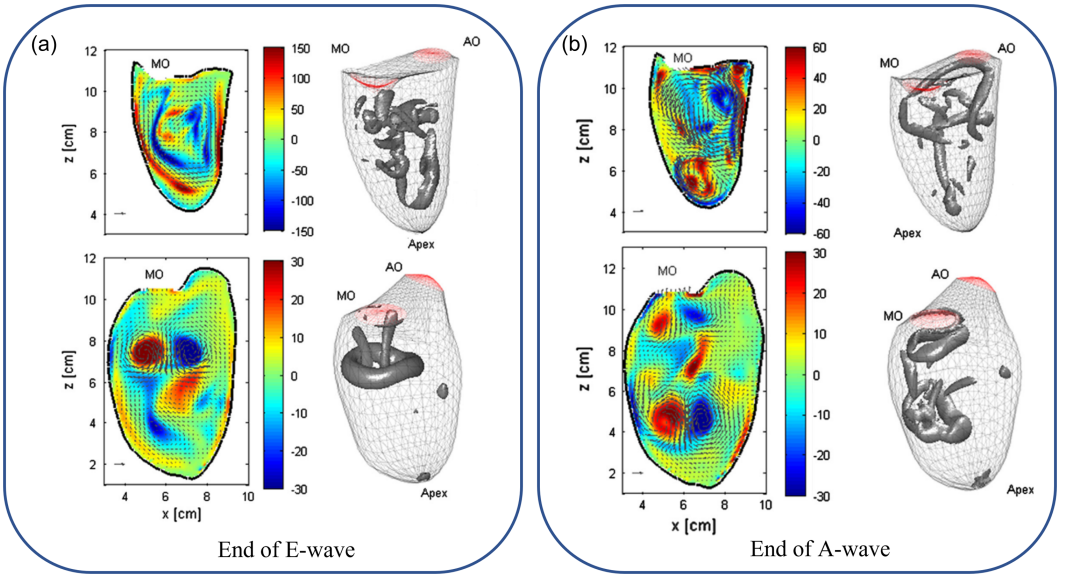

Figure 5. *Numerical simulations for diastolic intraventricular flow at the end of (a) E-wave and (b) A-wave for a healthy (top) and DCM patient (bottom). Comparison of flow structure for healthy and DCM patient – left: velocity vectors at the midplane of LV; middle: three-dimensional vortex fields by iso-surface of λ_2) criteria. Adapted with permission from previously published numerical simulations (Mangual et al., 2013).*
Notes: AO: Aortic valve, MO: Mitral valve.

to abnormal diastolic LV filling. The ejection fraction (EF) can be expressed in terms of the VFN as in equation 2. Recently, it has been observed that dilated LV shows lower washout rates in comparison with normal ones (Goubergrits et al., 2022; Obermeier et al., 2022). The increased stagnation zones were observed in dilated LVs and these contribute to blood clot formation

$$VFN = \frac{4(1-\beta)}{\pi} \cdot \alpha^3 \cdot EF, \tag{2}$$

where β is the fraction of stroke volume in the LV obtained from the left atrium (LA) and can be expressed as equation 3

$$\beta = \frac{V_A}{EDV} = \frac{VTI_A \times \frac{\pi}{4} D_E^2}{EDV}, \tag{3}$$

where V_A is the blood volume that entered the LV during atrial contraction, EDV is the LV end-diastolic volume, VTI_A is the velocity–time integral of the A-wave and D_E is the effective diameter of the mitral orifice area.

The variable α is a purely geometric parameter of the LV, defined by

$$\alpha = \frac{EDV^{\frac{1}{3}}}{\overline{D}}, \tag{4}$$

where EDV is the LV end-diastolic volume and $\overline{D}$ is the time-averaged MV diameter defined in Equation 1.

A comparison of intraventricular flow fields in healthy and DCM patients shows significant differences in velocity profiles, and three-dimensional flow fields, as shown in Figure 5 (Mangual et al., 2013). They have performed the simulation for one cardiac cycle on three-dimensional echocardiographic LV data acquired at a frame rate of 20–30 Hz. They were simulated using the immersed boundary method, and the Eulerian–Lagrangian approach was used to model wall movement and fluid flow. In this

https://doi.org/10.1017/flo.2025.6 Published online by Cambridge University Press

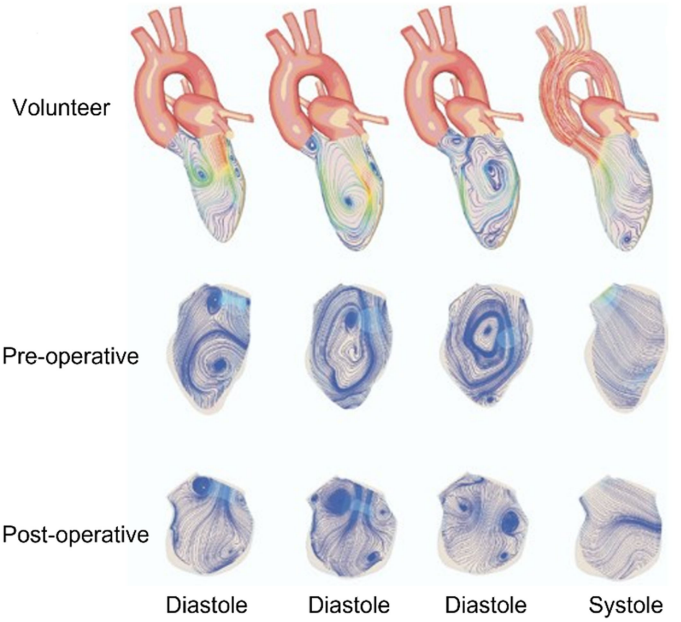

Figure 6. *Karlsruhe heart model simulations showing a comparison of vortex patterns in DCM models (pre-operative and post-operative) as opposed to a healthy model. Adapted with permission from previously published numerical simulations (Doenst et al., 2009).*

approach, the LV model is immersed inside the computational domain and inflow/outflow velocity profiles are automatically ensured by mass conservation from the system of equations. The flow patterns are shown at the end of the E-wave and A-wave diastolic phases, providing an important understanding of flow patterns in healthy and DCM patients. In the healthy LV, anticlockwise rotation of the vortex dominates the central cavity of the LV. However, diseased (DCM) LVs show a more complex vortex pattern in the middle of the LV (Figure 5: bottom). The three-dimensional flow structures visualised by the velocity gradient tensor (λ_2) criterion differentiate that the vortex is more stretched towards the apex in the healthy case as compared with a more compact vortex in a DCM patient. The vortical circulation is restricted to the central cavity in DCM patients, while it is well distributed in healthy subjects. The vortex strength is higher in healthy cases as compared with DCM patients, as shown in Figure 5. The vortex core is very compact and limited to the central LV cavity for DCM patients.

Note also that the presence of stagnation regions in a diseased case is prone to thrombus formation and leads to dangerous situations. A thrombus may propagate through the arteries and cut off blood supply in narrower arteries leading to further complications. A well-distributed blood flow throughout the LV indicates a healthy flow pattern.

Various studies simulated healthy and diseased LV models and compared vortex patterns to understand the changes in the vortex dynamics. Patient-specific LV models have been simulated by considering resistance and compliance/flexibility of arteries. Healthy and DCM LV models have been simulated and compared with the vortex patterns before and after surgery of DCM LV models, as shown in Figure 6 (Doenst et al., 2009). In a healthy LV, the asymmetric vortex is formed just after the MV opening, which was shown by CFD (Figure 6). The asymmetry might help to minimise the dissipative interaction between inflow, vortical structures and outflow (Kilner et al., 2000). The vortex ring is pinched off and rotated in a clockwise direction to redirect the flow toward the aorta. In the dilated LV (pre-operative case), dilation at the apex of LV deforms the vortex towards dilated regions which causes momentum loss during diastole. Similar flow structures were observed during systole for healthy and DCM cases.

https://doi.org/10.1017/flo.2025.6 Published online by Cambridge University Press

After the removal of the dilated region at the LV apex, the vortex deformation was reduced and blood flowed more efficiently toward the aorta with lower dissipation or losses.

As we have discussed so far there has been a systematic effort to study the vortex dynamics in the LV and its linkage to disease progression; also, a vortex formation index has been proposed. Table 1 shows the models, methods used and limitations for various LV numerical studies, Table 2 shows the experimental (*in vivo* and *in vitro*) methods and imaging techniques used in past studies with major outcomes, and Table 3 presents the relevant numerical studies and their outcomes on the whole heart and LV hemodynamics. However, this approach has not yet gained acceptance in clinical practice, since CFD modelling presents several limitations for various LV numerical studies, and more consistency in CFD outputs in various studies is desired to gain confidence for clinical practice. Consistency in results can be achieved by sharing models and methodology used in open-source platforms so that other researchers can utilise and replicate the results.

3. Challenges and opportunities in CFD modelling of the patient-specific left ventricle

The typical pipeline for patient-based modelling blood flow in the LV is sketched in Figure 7. This pipeline proceeds through stages, each of them with its own complications. The first stage is to collect the medical images (CT or MRI) of heart models from physicians. The images need to be segmented for extraction of the heart surface and further smoothing. The extracted model is fed to either open-source or commercial tools for mesh generation and simulation. Mesh independence tests are crucial before performing final simulations. After mesh independence assessment, the appropriate patient-specific boundary conditions are enforced for the heart model such as inlet flow/pressure profiles and ventricle wall movement. The blood flow dynamics in the heart model is simulated by solving numerically the Navier–Stokes equations. After solving the flow field, the three-dimensional vortical structures and various hemodynamic parameters can be extracted for flow analysis. The most used marker for heart health is the vortex structure and the VFN. These markers can be helpful in monitoring heart health and can also be beneficial for heart surgery planning or evaluation of post-surgery outcomes. Every step involved in a pipeline of blood flow modelling is further discussed in depth below.

3.1 Segmentation of heart models using medical images

The DICOM file format is commonly used in medical images for visualisation, transfer and segmentation purposes. The segmented models can be exported in stereolithography file formats for further processing, refinement and numerical simulations. The segmentation step involves generation of the endocardial surface and definition of the endocardial displacement field during systolic filling dilation. Plenty of tools are available for segmentation of medical images. However, the most popular tools are discussed in this section. The entire segmentation procedure can be performed using the open-source software 3D slicer (Kikinis et al., 2013), the vascular modeling toolkit (vmtk) (Antiga et al., 2008), vmtk features can be enhanced by using additional tools for cardiac surface processing and the SimpleElastix library for image processing (Fedele and Quarteroni, 2021; Klein et al., 2010). The segmented and processed models can be visualised using ParaView, an open-source visualisation software (A. Henderson, 2007). Although the above mentioned libraries are available, the segmentation and generation of whole heart model geometry with its moving endocardial walls and heart valves is a cumbersome and challenging task.

The accurate segmentation and reconstruction of heart models and their time-resolved wall motion using cine-MR or ultrasound images enhances diagnostic accuracy and CFD modelling credibility. However, due to the limitation of imaging resolution, a lack of accuracy in the imaging of the heart valves and ventricular apex is observed. The wall motion in very short time intervals during a cardiac cycle is difficult to resolve properly due to the limitation of temporal resolution in imaging modalities.

https://doi.org/10.1017/flo.2025.6 Published online by Cambridge University Press

Table 1. *Vortex dynamics studies using numerical methods in either the whole heart or LV models*

First Author and year	LV Model	Flow type	Viscosity model	Boundary condition	CFD Solver	Major limitations
(Fedele et al., 2023)	3-D PS heart	Turbulent	Newtonian	LP BC	In-house code	Newtonian blood
(Korte et al., 2023)	3-D PSLV healthy	Turbulent	Newtonian	Pulsatile IP	Ansys Fluent	Absence of MV, AV and LA chamber
(Bucelli et al., 2023)	3-D PSLV healthy	Turbulent	Newtonian	LP BC	In-house code	Newtonian blood
(Bennati et al., 2023)	3-D PSLV MVR	Turbulent	Newtonian	Pulsatile IP	OS solver	Newtonian blood, absence of EPL
(He et al., 2022)	3-D PSLV healthy	Laminar	Newtonian	Pulsatile IP	Ansys Fluent	Absence of MV, AV, and LA chamber
(Grünwald et al., 2022)	3-D PSLV healthy	Turbulent	Non-Newtonian	Pulsatile IP	Ansys Fluent	Absence of MV, AV, and LA chamber
(Colorado-Cervantes et al., 2022)	3-D PSLV healthy	Laminar	Newtonian	Pulsatile IP	COMSOL	Absence of MV, AV, and LA chamber
(Collia et al., 2022)	3-D PSLV & ILV healthy	Laminar	Newtonian	Pulsatile IP	In-house code	Absence of LA chamber
(Meschini et al., 2021)	3-D ILV, healthy	Laminar	Newtonian	Pulsatile IP	OS solver	Ideal model, absence of LA chamber
(Collia et al., 2021)	3-D PSLV healthy	Laminar	Newtonian	Pulsatile IP	In-house code	Absence of LA chamber
(Viola et al., 2020)	3-D ILV, healthy	Laminar	Newtonian	Pulsatile IP	OS solver	Ideal model
(Lantz et al., 2019)	3-D PSLV, healthy	Laminar	Newtonian	Pulsatile IP	Ansys CFX	Absence of moving MV & AV
(Chan et al., 2019)	3-D ILV, healthy	Laminar	Newtonian	Pulsatile IP	COMSOL	Absence of moving MV & AV
(Meschini et al., 2018)	3-D ILV, healthy	Laminar	Non-Newtonian	Pulsatile IP	OS solver	Ideal model, absence of LA chamber
(Tagliabue et al., 2017a)	3-D ILV, healthy	Laminar	Newtonian	Pulsatile IP	OS solver	Ideal model & absence of LA chamber
(Gao et al., 2017)	3-D PSLV healthy	Laminar	Newtonian	Pulsatile IP	OS solver	Absence of moving AV
(Domenichini and Pedrizzetti, 2016)	3-D ILV, healthy	Laminar	Newtonian	Pulsatile IP	In-house code	Ideal model, absence of moving MV & AV

Table 1. *continued*

First Author and year	LV Model	Flow type	Viscosity model	Boundary condition	CFD Solver	Major limitations
(Liao et al., 2016)	3-D PSLV, DCM	Laminar	Newtonian	Constant Inlet	Ansys Fluent	Static LV & constant inlet.
(Vedula et al., 2015)	3-D PS left heart model	Laminar	Newtonian	Pulsatile IP	In-house code	Absence of moving MV
(Song and Borazjani, 2015)	3-D PSLV, healthy	Laminar	Newtonian	Pulsatile IP	In-house code	Absence of MV, AV & LA chamber
(Khalafvand et al., 2015)	2-D PSLV & MMV	Laminar	Newtonian	Pulsatile IP	Ansys Fluent	2-D geometry, absence of LA chamber & AV
(Seo et al., 2014)	3-D PSLV, PS	Laminar	Newtonian	Pulsatile IP	In-house code	Absence of AV & LA chamber
(Vedula et al., 2014)	3-D ILV & healthy	Laminar	Newtonian	Pulsatile IP	In-house code	Ideal model, Absence of MV and AV
(Chan et al., 2013a)	2-D ILV & DCM	Laminar	Newtonian	Pulsatile IP	COMSOL	Ideal 2-D axisymmetric Newtonian
(Chan et al., 2013c)	2-D ILV & DCM	Laminar	Newtonian	Pulsatile IP	COMSOL	Ideal 2-D axisymmetric Newtonian
(Mangual et al., 2013)	3-D PSLV healthy	Laminar	Newtonian	Pulsatile IP	In-house code	Absence of MV, AV & LA chamber
(Zheng et al., 2012)	3-D ILV & healthy	Laminar	Newtonian	Pulsatile IP	In-house code	Ideal model, Absence of MV and AV
(Doenst et al., 2009)	3-D PS left heart model	Laminar	Cross-model	Pulsatile IP	In-house code	Absence of MV, AV & PS BCs
(Schenkel et al., 2009)	3-D PSLV healthy	Laminar	Cross-model	Pulsatile IP	Star-CD	Absence of MV, AV & LV chamber
(Loerakker et al., 2008)	2-D ILV & DCM	Laminar	Newtonian	Pulsatile IP	In-house code	Ideal 2-D axisymmetric Newtonian

Table 1. *continued*

First Author and year	LV Model	Flow type	Viscosity model	Boundary condition	CFD Solver	Major limitations
(Domenichini et al., 2007)	3-D ILV & healthy	Laminar	Newtonian	Pulsatile IP	In-house code	Ideal model, Absence of MV and AV
(Pedrizzetti and Domenichini, 2005)	3-D ILV & healthy	Laminar	Newtonian	Pulsatile IP	In-house code	Ideal model, Absence of MV and AV
(Domenichini et al., 2005)	3-D ILV & healthy	Laminar	Newtonian	Pulsatile IP	In-house code	Ideal model, Absence of MV and AV
(Cheng et al., 2005)	3-D ILV & healthy	Laminar	Newtonian	Pulsatile IP	ADINA-FSI	Ideal model, Absence of MV and AV
(Baccani et al., 2002b)	2-D ILV & DCM	Laminar	Newtonian	Pulsatile IP	In-house code	2-D axisymmetric, Laminar, Newtonian
(Baccani et al., 2002a)	2-D ILV & healthy	Laminar	Newtonian	Pulsatile IP	In-house code	2-D axisymmetric, Laminar, Newtonian
(Vierendeels et al., 2000)	2-D ILV & healthy	Laminar	Newtonian	Pulsatile IP	In-house code	2-D axisymmetric, Laminar, Newtonian

Notes: IP = inlet profile; DCM =dilated cardiomyopathy; ILV = ideal left ventricle; PSLV = patient-specific left ventricle; MV = mitral valve; AV = Aortic valve; PS = Patient-specific; BC = boundary condition; MMV = moving mitral valve; OS = open source; MVR = mitral valve regurgitation; EPL = electrophysiology; Ansys Fluent, (ANSYS, 2022) COMSOL (COMSOL, 2018).

Table 2. *Vortex dynamics studies using experimental techniques in the LV models*

First author & year	Experimental Technique	Imaging modality	Major outcomes
(Becker et al., 2023)	VFM (*In vivo*)	ECGP	The growing heart undergoes a transition to an adult vortex pattern over the first 2 years with higher loss
(Njoku et al., 2022)	4-D flow MRI (*In vivo*)	4-D MRI	4-D flow MRI is better for mitral flow analysis as compared with Doppler ECGP
(Di Labbio et al., 2022)	D-PIV (*In vitro*)	High-speed camera	Proposed flow topologies using braid for healthy & diseased LV & can be a measure of outcomes
(Hu et al., 2022)	4-D flow CMR	4D CMR	The space needed for optimal vortex formation is observed in children and adults between 6 and 18 years
(Gülan et al., 2022)	4-D flow MRI	4D MRI	Low shear stresses in the ventricle denote higher adaptability to blood flow & increased compliance
(La Gerche et al., 2022)	S-T ECGP (*In vivo*)	3D ECGP	Young athlete hearts can generate greater outputs with lesser resting volume.
(Monosilio et al., 2022)	S-T ECGP (*In vivo*)	2D ECGP	Patients with heart failure by reduced EF show lower & misaligned hemodynamic forces
(Zhang et al., 2021)	ECGP (*In vivo* & *In Vitro*)	ECGP	LV dysfunction had lower vorticity & strain in comparison with the healthy group
(Yang et al., 2021)	VFM (*In vivo*)	CD ECGP	DCM LV affects the direction of vortex rotation & can be a good indicator for detection
(Wiener et al., 2021)	PIV (*In vitro*)	ECGP	Stenosed MV increases transmitral gradients, but increased VED during exercise
(Adabifirouzjaei et al., 2021)	VFM (In vivo)	CD ECGP	The degree of diastolic energy loss is directly proportional to the level of Transmitral flow velocity
(Matsuura et al., 2019)	VFM (*In vivo*)	Doppler ECGP	Peak E vorticity was strongly related to intra-ventricular pressure difference in a healthy dog's LV
(Han et al., 2019)	VFM (In vivo)	CD ECGP	Healthy LV shows apically directed flow & severe cases shows bidirectional flow with small vortices
(Berlot et al., 2019)	VFM (*In vivo*)	CD ECGP	Apical intraventricular velocity gradient was lowest in control groups in comparison with DCM
(Labbio and Kadem 2018)	TR-PIV (*In vitro*)	High-speed camera	Diastolic vortex reversal was observed in LV & an increase in energy dissipation in AR severities

https://doi.org/10.1017/flo.2025.6 Published online by Cambridge University Press

Table 2. *continued*

First author & year	Experimental Technique	Imaging modality	Major outcomes
(Chan et al., 2017)	Adaptive vectors	PC-MRI	Flow propagation velocity is affected by jet direction & measurement location.
(Stugaard et al., 2015)	VFM (*In vivo*)	CD ECGP	Diastolic energy loss increases in AR proportional to its severity & can be a marker for severity of AR
(Bermejo et al., 2014)	2-D Doppler colour-*In vivo*	PC-MRI	Patients with DCM shows larger & stronger vortices as compared with healthy patients
(Fortini et al., 2013)	D-PIV (*In vitro*)	High-speed camera	The asymmetric single vortex is generated & its coherence is not broken by second filling.
(Eriksson et al., 2013)	4-D flow MRI (*In vivo*)	MRI & ECGP	DCM results into altered diastolic flow routes and impaired preservation of inflow KE at pre-systole
(Abe et al., 2013)	E-PIV (*In vivo*)	ECGP	The change in vortex strength is related to LV performance.
(Stewart et al., 2012)	Echo Doppler	Pc – MRI	Vortex ring pinch-off occurs before the completion of early diastole and is independent of diastolic function.
(Kheradvar et al., 2012)	ECGP (*In vivo*)	ECGP	Mitral annulus velocity was lower in abnormal cases. VFT varies in normal & abnormal cases
(Kheradvar et al. 2010)	E-PIV & D-PIV (In vitro)	Camera & ECGP	Flow patterns obtained using E-PIV & D-PIV are comparable & E-PIV limits small-scale features
(Kheradvar and Gharib, 2009)	PFS (*In vitro*)	Catheter & sensors	Transmitral thrust is maximum when VFT is in range of 4-5.5 & it can be an index of LV health
(Kheradvar and Gharib, 2007)	D-PIV (*In vitro*)	High-speed camera	The magnitude of recoil is maximum during vortex pinch-off & VFT range of 3.5–4.5
(Pierrakos and Vlachos, 2006)	D-PIV (*In vitro*)	High-speed camera	The critical value of VFN for healthy LV is 6. Vortex formation depends on valve design.

Notes: D-PIV = particle image velocimetry; E-PIV = Electrographic particle image velocimetry,; TR = time-resolved; CD = colour Doppler; S-T = speckle-tracking; ECGP = echocardiography; pc-MRI = phase-contrast MRI; MRI = magnetic resonance imaging; VFM = vector flow mapping; PFS = pulse flow simulator; VFN = vortex formation number; VFT = vortex formation time; AR = aortic regurgitation; VED = viscous energy dissipation; EF = ejection fraction; CMR = cardiovascular magnetic resonance.

The number of frames per cardiac cycle is limited to 20–30. The intermediate surfaces between very short intervals of time are obtained by interpolation of temporal datasets (Antiga et al., 2008; Renzi et al., 2023).

Regarding the segmentation techniques, two main approaches exist: image-driven approaches and model-driven approaches. Image-driven models are designed without or with weak prior models, while model-driven approaches are based on strong prior knowledge. The image-driven approach identifies the

https://doi.org/10.1017/flo.2025.6 Published online by Cambridge University Press

Table 3. *Major contributions from recent CFD studies to vortex dynamics in patient-based whole heart or LV models and important outcomes*

First author & year	Important outcomes
(Fedele et al., 2023)	Modelled electromechanical model of the whole human heart that considers both atrial and ventricular contraction with myocardial architecture. Model able to reproduce healthy cardiac functions.
(Bucelli et al., 2023)	Provides 3-D representation of cardiac muscles and hemodynamics using FSI. They included cardiac electrophysiology, active and passive mechanics and hemodynamics.
(Bennati et al., 2023)	Modelled left heart in the presence of MVR with MV movement and observed rise in regurgitant jets through the mitral orifice impinging against the atrial walls leads to increased WSS compared with healthy case.
(Korte et al., 2023)	Patient-specific simulations show lower systolic KE during exercise in comparison with rest. Precise segmentation of moving LV is crucial for better accuracy.
(Grünwald et al., 2022)	Modelled patient-specific wall movement in LV for SRV and healthy cases. They found out reduced value of VFT and total KE in SRV patients. Vortex circulation is limited to centre of the LV which leads to a reduction in washout of SRV patients.
(Lantz et al., 2019)	Performed intracardiac blood flow simulations in LV by varying inlet velocity profiles at pulmonary veins. Large differences in flow patterns observed in LA and negligible differences for LV at various inflow profiles.
(Mao et al., 2017)	A fully coupled FSI approach is used for modelling MV and AV movement and its effect on hemodynamics. A comparison of FSI results with a LV model without valves shows a significant difference in the flow field. The FSI approach is close to physiological values.
(Gao et al., 2017)	Numerical simulations are performed for the MV-LV model using nonlinear soft tissue mechanics of MV. This methodology shows good agreement with physiological values such as aortic flow rate, end-systole and end-diastole ejection fractions.
(Vedula et al., 2015)	Investigated flow pattern in LA and its effect on LV hemodynamics using medical images. A comparison of the ventricle flow velocities between the physiologic and simplified LA model shows a difference of approximately 10 % of peak mitral velocities.
(Pasipoularides et al., 2015)	Clinical validation is needed to support the VFN as a marker for LV diastolic function. The VFN as originally proposed cannot be used as an index of ventricular diastolic function.
(Mangual et al., 2013)	Comparative analysis of hemodynamics is performed between health and dilated LV models. Reduction of energetic efficiency and increase of flow stagnation is observed in DCM cases.

Notes: FSI = fluid-structure interaction; MVR = mitral valve regurgitation; WSS = wall shear stress; KE = kinetic energy; LV = left ventricle; SRV = single right ventricle; VFT = vortex formation time; AV = aortic valve; MV = mitral valve.

https://doi.org/10.1017/flo.2025.6 Published online by Cambridge University Press

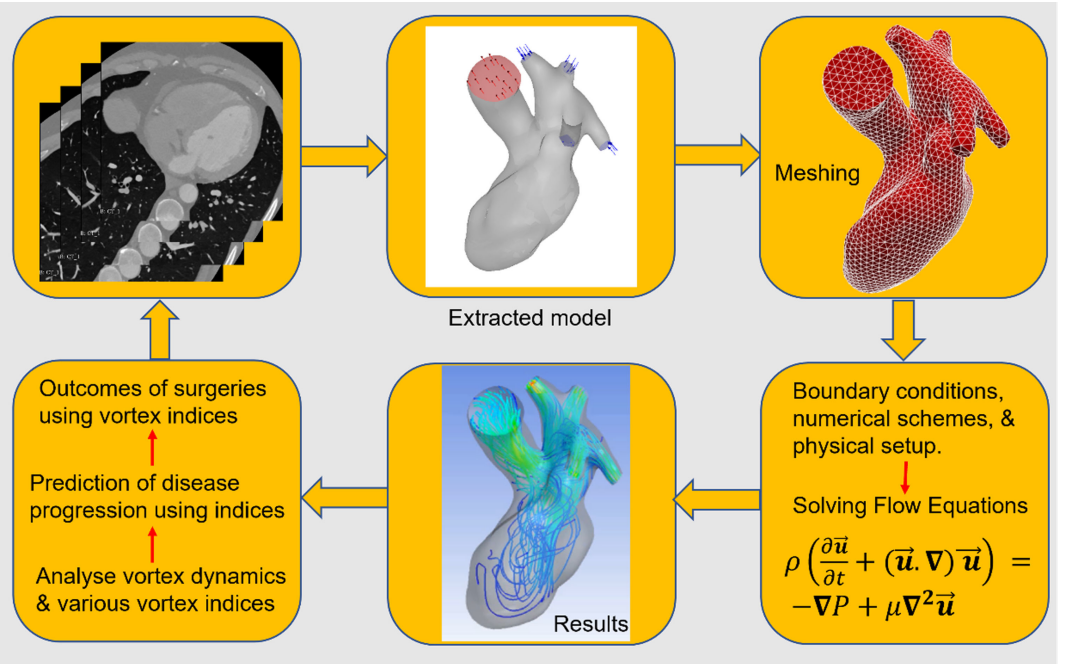

Figure 7. *Pipeline used in CFD modelling of vortex dynamics in patient-specific left heart model.*

pixel difference in tissue, blood pool and myocardium and segmentation can be performed by thresholding and region-growing methods (Peng et al., 2016). On the other side, a model-driven approach uses strong prior knowledge about the specific shape variability of the ventricle chambers, instead of making assumptions on boundaries. Various researchers have used a model-based approach for segmentation of the heart and this method has shown promising results (Mitchell et al., 2002; van Assen et al., 2006).

Choice of segmentation techniques is not trivial and can be constrained by the specific protocol. Model-based technique can be useful for obtaining LV walls combined with thresholding to eliminate the effect of papillary muscles. If training datasets are limited, then the use of model-based techniques is not preferred, and it is instead advised to refer to image-driven approaches. Finally, segmentation accuracy is the major criterion for selecting a segmentation technique.

Challenges of whole heart segmentation are mainly due to large shape changes of the heart and unclear boundaries between various substructures. A practical problem is the computational time for segmentation raised from a non-rigid registration process. Other challenges that arise in the use of fully automatic algorithms are large variability of the heart shape, indistinct boundaries and restricted image quality or resolution. The automatic algorithms cannot be applied to every heart simulation, but rather they are limited to specific tasks.

3.2 Numerical scheme consistency

We observed a disparity in various numerical schemes used for modelling of LV hemodynamics. Few studies used first-order temporal or spatial discretisation, while others have used second- or higher-order discretisation methods. Similarly, different pressure–velocity coupling schemes have been used in past studies. It is not clear which order of discretisation or pressure–velocity coupling is best for biomedical simulations. Sufficient knowledge of various numerical schemes and their effect on vortex patterns in the LV would be a great guide for *in silico* medicine. However, most of the studies used second-order schemes for temporal discretisation and second- or higher-order schemes for spatial discretisation. Nowadays, the use of higher-order schemes in industrial applications is a common practice.

https://doi.org/10.1017/flo.2025.6 Published online by Cambridge University Press

The appropriate choices on use of numerical schemes with the *in vivo* or *in vitro* validation can be an excellent addition to available literature knowledge. A universal guide for CFD methods used and consistency in results obtained could be a better approach to translating CFD results into clinical decisions. The successful adaption of CFD to clinical decision making can be possible when CFD output is readily tuned for specific clinical needs.

3.3 Boundary condition specification

The effect of boundary conditions on flow patterns and hemodynamic markers have been thoroughly studied and shows the necessity of using individual patient-specific boundary conditions (Dahl et al., 2012; Lantz et al., 2019). Numerical results significantly depend on the accuracy of boundary conditions. Inappropriate boundary conditions lead to incorrect prediction of flow fields and hemodynamic markers (Tagliabue et al., 2017b). Use of generic boundary conditions available in commercial solvers restricts the use of CFD analysis in medical practice due to deviations from *in vivo* physiology. However, a recent study explored the effect of various inlet boundary conditions on hemodynamics and advised that artificial inlet profiles are acceptable to use in the absence of patient-specific boundary conditions (Wei et al., 2019). Artificial inlet profiles are generic inlet boundary conditions adapted from literature studies which consist of an E-wave and A-wave (diastolic filling), as shown in Figures 4 and 8(b). The inlet profile is similar in all healthy cases, but it can be different in diseased cases (Wei et al., 2019). Patient-specific inlet boundary conditions are replications of *in vivo* velocity/flow profiles measured by phase-contrast MRI or catheterisation. Using such inlet profiles in CFD simulation for each patient-specific LV replicates the CFD results close to *in vivo* flow patterns. The flow profiles obtained from medical data can be implemented in CFD simulations by interpolating the flow curve and writing a customised function (e.g. in Ansys, a user-fefined function) for boundary condition implementation. Note that obtaining the blood flow velocities or pressure at various valve locations is not a routine clinical practice, which limits the availability of patient-specific boundary conditions and accurate flow dynamics in the heart. It can be a very good initiative to perform whole heart simulations using patient-specific flow and wall properties. Patient-specific flow profiles at specified regions can be obtained using four-dimensional flow MRI studies. Similarly, computed tomography angiography (CTA) with Doppler ultrasound can be used to extract two-dimensional velocity profiles at desired planes. These extracted profiles from clinical data can be implemented into CFD simulations using curve fitting and extracting the coordinates. Patient-based wall properties can be acquired using tagged MRI which provides detailed strain and wall deformation of the LV. Similarly, three-dimensional echocardiography gives a volumetric view of heart wall motion. High-resolution MRI measures the thickness of the heart muscles. While speckle tracking echo measures wall strain in real time. Measured principal strains from tagged MRI can be validated with experimental stress tests. These tests consist of tensile tests to obtain a stress–strain curve, biaxial testing to calculate anisotropic properties and shear tests for measuring the shear modulus and viscoelastic behaviour. Hyperplastic models can be implemented to model heart muscle behaviour, The Holzapfel–Ogden model accounts for anisotropy and could be beneficial over isotropic models. Such studies will add valuable knowledge to the existing literature, and it will be possible to translate such studies into clinical practices.

We have simulated and compared the effect of plug and parabolic inlet profiles on vortex formation and found that vortex patterns are significantly different, as shown in Figure 9(d). The vortex patterns obtained using a plug flow inlet is in agreement with *in vivo* flow dynamics and past published articles (Chan et al., 2013c). Therefore, it is recommended to use the plug inlet profile at the LV inlet (MV) during LV filling simulations. In a recent study, three different models of left heart models with varying inlet pulmonary veins (PVs) were compared and analysed (Dahl et al., 2012). Four jets enter the atrium asymmetrically, and complex vortex patterns are observed. They found that, with anatomically based PV positions, the flow was directed towards the MV without collision. This model shows an evenly distributed velocity at the MV plane and lower maximum transmitral velocity during the E-wave. The asymmetrically located veins prevent flow instabilities and excessive energy dissipation in the flow. To

https://doi.org/10.1017/flo.2025.6 Published online by Cambridge University Press

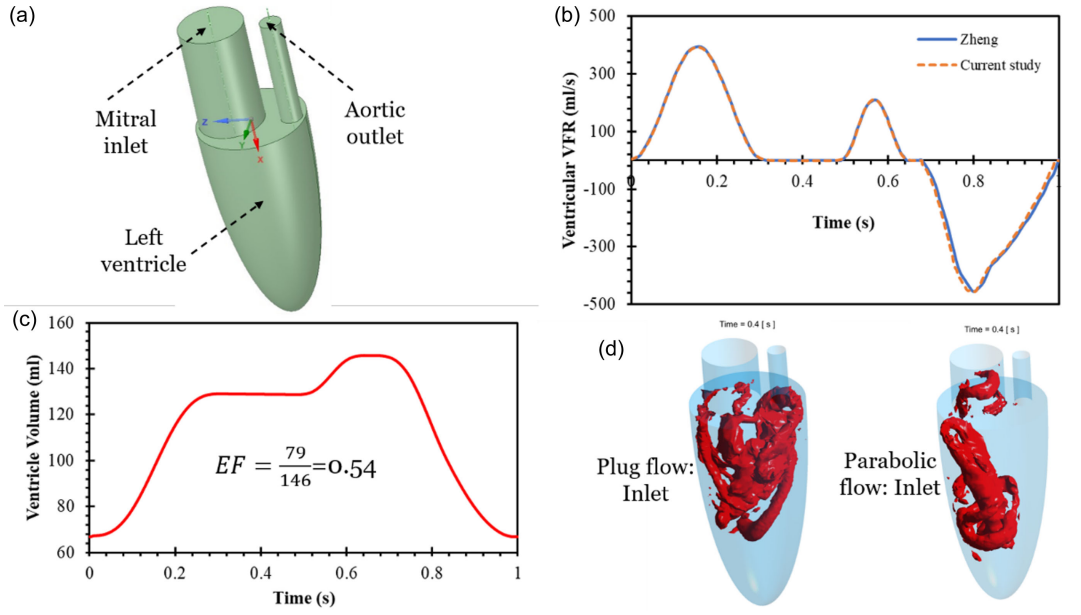

Figure 8. *Validation and comparison of inlet flow profiles with Zheng et al. (2012) using moving mesh methodology: (a) ideal geometry of LV, (b) validation of ventricular VFR with past study, (c) ventricle volume change during cardiac cycle, (d) fffect of plug and parabolic inlet profile on Q-criterion in ideal LV model.*

obtain physiologically correct simulations, ventricular filling and MV dynamics should be modelled using patient-specific anatomies, flow rates and MV properties. In another recent study, three different inlet waveforms at the PVs are analysed using four-dimensional flow MRI (Lantz et al., 2019). They have observed that different inlets at PVs affect the LA flow patterns. A large variation in kinetic energy (KE) is observed for varying inlet velocity profiles, especially during the early filling phase. *In vivo* MRI measurement shows higher flow volumes on the right side of PVs compared with the left side, which seems to be realistic as the right lung has three lobes and the left lung has only two lobes. Some of the vortical structures generated in the LA transferred towards the LV. The high residence time regions trigger thrombus formation and it is most commonly observed at abnormal flow regions in the LA (Hara et al., 2009; Heppell et al., 1997). Asymmetrical filling of the LA preserves the momentum and is redirected towards LV through the MV (Kilner et al., 2000).

3.4 Wall modelling

Moving mesh methods are useful for simulating the large expansion characterising the movement of the LV walls. A possible implementation of a moving mesh approach interprets interpolating the LV surface generated at various time instances during a cardiac cycle. The change in LV volume is reconstructed from medical images in spatio-temporal node positions. The mesh is updated to respective dilated LV volume using surface coordinates at various time instances. It is very difficult to use two-way fluid–structure interaction (FSI) for larger deformations of the LV. However, FSI is useful for modelling heart valve movement. In the FSI, the momentum transfer from fluid (blood) to solid (artery wall/endothelial surface) and *vice versa* is modelled. Current spatial and temporal resolutions for cardiac MRI are around 1–1.5 mm and 40–50 ms, respectively (Saeed et al., 2015). This resolution is inadequate to capture the motion of heart valves. Very few studies have modelled patient-specific heart models with heart valve movement (Chnafa et al., 2014; Gao et al., 2017; Mao et al., 2017; Seo et al., 2014; Su et al., 2014, 2016).

https://doi.org/10.1017/flo.2025.6 Published online by Cambridge University Press

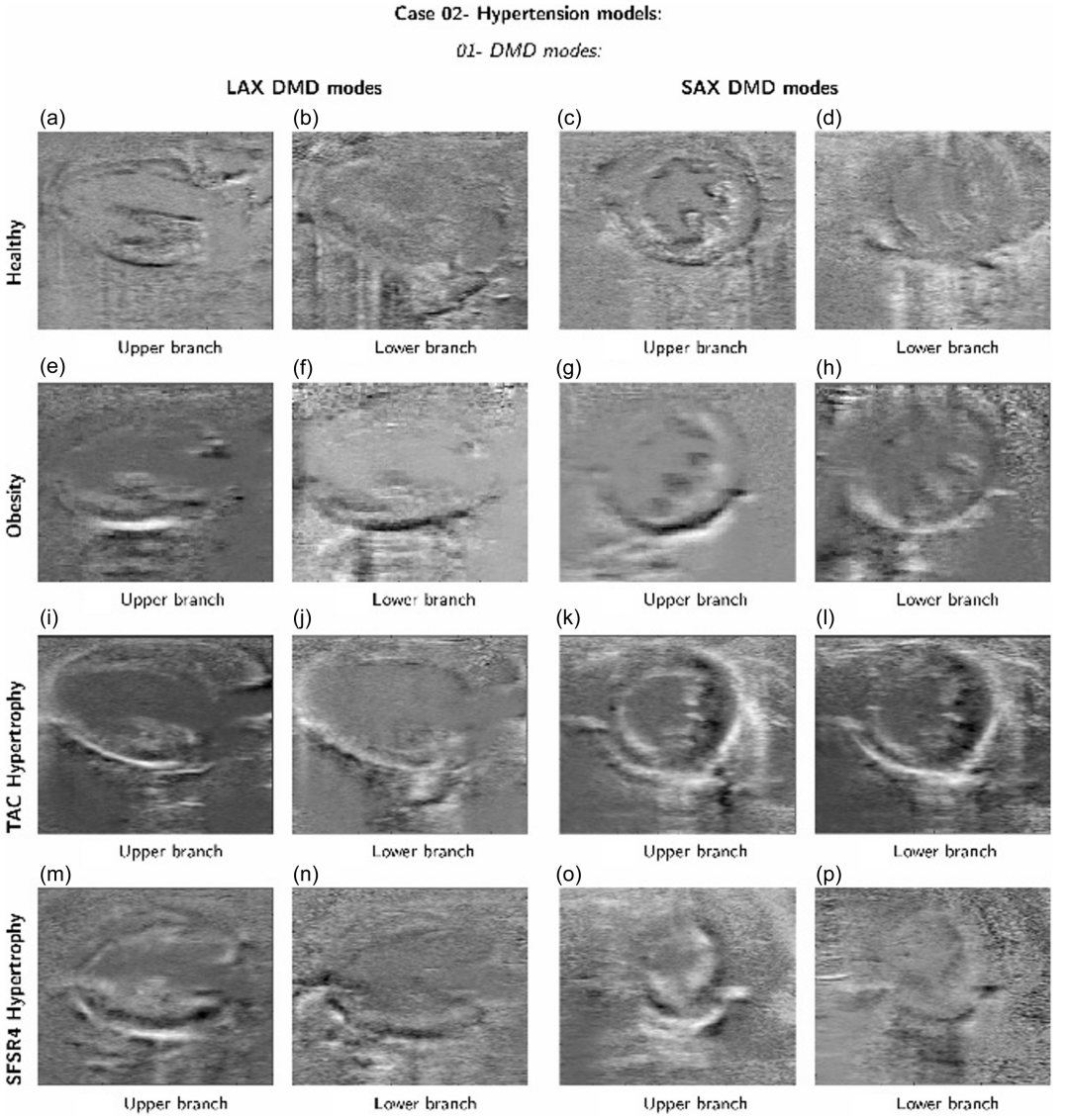

Figure 9. *A comparison between the DMD modes obtained from the healthy data set and the DMD modes obtained from analysing the datasets of the hypertrophic hearts. Reproduced from (Groun et al., 2022).*

Notes: TAC: Time-Area Curves, SFSR4: Segmental Function Score for Radial 4-Chamber, LAX: Long-Axis and SAX: Short-Axis Views.

In most of the studies, valves are modelled as either fully open or fully closed; moreover, valve opening and closing are assessed to be very fast, almost instantaneous. However, neglecting wall movement during opening and closing may affect the left ventricular flow patterns. Valve movement has been modelled in two ways, either using medical imaging data to specify opening and closing motion or directly simulating using the FSI approach. It is necessary to give wall boundary conditions during early diastole to the aortic valve and during systole to the MV. Specifying the wall boundary condition defines the valve as completely closed. These can be changed during a cardiac cycle from wall to velocity inlet or pressure outlet and *vice versa*. Specifying these boundary conditions replicates the opening and

https://doi.org/10.1017/flo.2025.6 Published online by Cambridge University Press

closing of valves during the diastole and systole phases of the cardiac cycle. Despite many investigations having been conducted by using different types of boundary conditions for LV valves, it is still unclear what is the best fit of boundary conditions to replicate physiological flow features in the LV. The best practice to model the valves is to use the FSI approach instead of modelling it as completely open or closed. The FSI approach is computationally expensive and time consuming. It can be modelled using a computationally viable moving mesh approach, but we need surface information on valve movement. However, it is difficult to extract valve movement due to current imaging constraints. The opening and closing of valves are so rapid that current imaging techniques will not be helpful in extracting their movement. After extracting valve movement, it can be modelled using the moving mesh approach which has been used in modelling LV wall movement.

3.5 Newtonian and non-Newtonian blood models

It has been argued that blood flow in larger arteries and veins can be modelled as Newtonian (Ku, 1997). The heart is, in a sense, a large vessel, but it involves complex flow patterns due to contraction and expansion of endocardial walls and moving heart valves. The flow patterns in the heart chamber involve vortices and recirculation. The recirculation leads to lower shear rate values, and it is well known that blood viscosity is dependent on local shear rates (Cho and Kensey, 1991). The lower shear rate leads to increased blood viscosity, and it becomes important to understand the effect of non-Newtonian models on vortex patterns in the LV. A recent study attempted to investigate the effect of various non-Newtonian models (shear thinning) on vortex analysis in the LV and they found a significant difference between both vortex patterns and vortex ring angle in various non-Newtonian models (Doost et al., 2016b). The number of smaller vortices and their magnitudes are different for various non-Newtonian models. A larger apparent viscosity value is observed in the apex and middle of the LV. The vortex patterns are the major marker of measuring heart function, and it shows the importance of non-Newtonian blood flow modelling in the LV. They have analysed the effect of non-Newtonian blood for a single case. It would be interesting to see a comparison of non-Newtonian models in large datasets of patient-specific LVs, especially in DCM patients. In DCM patients, LV volume is increased and larger stagnation regions are observed which can lead to increased viscosity regions. To the best of the authors' knowledge, there is no study available on the effect of VFN for various non-Newtonian models in healthy and diseased LVs. The VFN has been considered as an important marker of identifying normal and abnormal vortex patterns in the LV. Overall, the consideration of non-Newtonian modelling becomes important due to its strong linkage with vortex patterns and the VFN.

Few other studies have investigated the effect of non-Newtonian models on the hemodynamics of mechanical heart valves and left-ventricular assist devices (Al-Azawy et al., 2017; De Vita et al., 2016). They found that, irrespective of having larger vessels such as the aorta and heart pump, shear rate values are lower than threshold limits to show constant viscosity and its shear-thinning behaviour might affect the flow patterns. Haemolysis, induced due to altered wall shear stress (WSS), is observed to be higher for the non-Newtonian model compared with Newtonian blood (De Vita et al., 2016). Further, it was suggested to use non-Newtonian models for modelling left ventricular-assisted devices. They found that the shear rate values are lower than 100 s^{-1} in the chamber and these shear rate values belong to the nonlinear viscosity range for blood (Al-Azawy et al., 2017). Total KE is observed to be higher for non-Newtonian models compared with Newtonian ones. Finally, there is insufficient knowledge available on which non-Newtonian model is the best fit for hemodynamics in the LV (De Vita et al., 2016). It would be a great addition to the literature to validate CFD vortex patterns using various non-Newtonian models with four-dimensional flow MRI vortex data. The closely matching non-Newtonian model can be recommended for future simulation to avoid confusion.

3.6 Validation of numerical methodology

Validation of numerical results against well-designed experimental datasets is necessary for gaining confidence in CFD simulations. The accuracy of CFD simulations in biomedical flows largely depends on

https://doi.org/10.1017/flo.2025.6 Published online by Cambridge University Press

the selection of geometry, boundary conditions, blood and wall properties, mesh quality and numerical methods used. Due to simplifications and assumptions made during heart simulations, it is very difficult to validate these results with experimental or *in vivo* data. Very few studies validated their CFD results against the experimental values. Vedula et al., have validated the hemodynamics in a moving LV model with particle image velocimetry experiments, which matched well both qualitatively and quantitatively (Vedula et al., 2014). Few other studies validated CFD results with *in vivo* flow profiles obtained using four-dimensional flow MRI and they matched qualitatively (Saber et al., 2003; Schenkel et al., 2009).

We have validated the numerical methodology with Zheng et al., on an idealLV hemodynamics, as shown in Figure 9 (Zheng et al., 2012). Simulations were performed using a well-established moving mesh approach. The movement of heart walls during diastolic filling has been mimicked by updating surface files in a short interval of time during simulations, please see section 3.4 for a more detailed explanation. Figure 9(a) shows the ideal LV model (Vedula et al., 2014), which is a semi-prolate ellipsoid in shape consisting of a mitral orifice (inlet) and aortic outlet. The inlet profile is adapted from the literature and compares the volumetric flow rate (VFR) at inlets and outlets and it has already been discussed in the boundary condition section. Figure 9(b, c) shows the validation of the ventricular VFR for the present simulation with Zheng et al., and the ejection fraction (ratio of ejected volume to the total LV volume) achieved matches their results (Zheng et al., 2012).

3.7 New tools for pattern identification

The identification of coherent structures is of paramount importance in the field of cardiac flow modelling. However, this area remains under-explored due to the inherent complexity of the problem. New data-driven techniques offer a promising avenue for advancing our understanding of the flow physics, providing general descriptions of the main mechanisms involved in heart dynamics, and detecting the presence and evolution of the vortex ring originated in early diastole from the MV.

For instance, data-driven modal decomposition techniques can identify the primary patterns and global instabilities driving the flow dynamics. Two prominent methods in fluid dynamics are proper orthogonal decomposition and dynamic mode decomposition (DMD). Proper orthogonal decomposition decomposes the flow into the most energetic orthogonal modes, representing large-scale structures. Dynamic mode decomposition identifies high-amplitude modes driving the flow dynamics. By identifying the main flow patterns, it is possible to connect these structures with healthy or diseased heart mechanisms, allowing for the preemptive detection of CVDs. These data analysis techniques have gained traction in medical image analysis and diagnosis (Fathi et al., 2018; Grinberg et al., 2009), extending to conditions like Parkinson's and lung disease (Fu et al., 2020; Xi and Zhao, 2019).

In particular, a study by (Groun et al., 2022) has investigated the use of higher-order dynamic mode decomposition (HODMD) in the realm of medical imaging, particularly in the analysis of echocardiography images obtained from mice with different cardiac conditions. The algorithm demonstrated robust performance, successfully capturing two branches of frequencies related to heart and respiratory rates across all datasets. Despite variations in the number of identified modes and frequencies due to noise level, disease characteristics and anaesthesia effects, HODMD consistently distinguishes characteristic patterns associated with each cardiac pathology, as shown in Figure 8.

Inspired by these results, in future avenues, we will apply the HODMD algorithm to analyse cardiac flow CFD databases, shedding light on vortical structures within the LV model. The data from this CFD simulations is compiled into a three-dimensional snapshot tensor called $\boldsymbol{v}(x, y, z, t_k)$, which we feed into the HODMD algorithm. This method decomposes the dataset into an expansion of DMD modes $\boldsymbol{u}_m$ each of them associated with an amplitude a_m, as

$$\boldsymbol{\upsilon}(x, y, x, t_k) \simeq \sum_{m}^{M} = 1 a_m \boldsymbol{u}_m(x, y, z) e^{(\delta_m + i\omega_m)t_k}$$

for $k = 1, \ldots, K$. The DMD modes can grow, decay or remain neutral according to the associated growth rate δ_m and oscillate in time with the frequency ω_m.

https://doi.org/10.1017/flo.2025.6 Published online by Cambridge University Press

Notably, this algorithm exhibits several advantages, including its capability to analyse three-dimensional data, integrate both experimental and numerical data sources and obtain a set of modes associated with the vortical structures.

Recent advances in deep learning, including convolutional neural networks (CNNs) and recurrent neural networks, have significantly enhanced our ability to manage and interpret the large datasets generated by improved cardiac flow simulations. These artificial intelligence (AI) and machine learning techniques have been instrumental in diagnosing CVDs, particularly through the classification of MRI image sequences of coronary arteries (Berikol et al., 2016; Worden et al., 2015).

The work by Bell-Navas et al. introduces an automatic cardiac pathology recognition system using a novel deep-learning framework (Bell-Navas et al., 2025). This system analyses real-time echocardiography video sequences in two stages. The first stage converts echocardiography data into annotated images suitable for machine learning, employing the HODMD algorithm for data augmentation and feature extraction. The second stage involves training a vision transformer from scratch, adapted for small datasets. This neural network predicts heart conditions from echocardiography images and has shown superior performance, even surpassing pre-trained CNNs, highlighting the efficacy of the HODMD algorithm in the medical field.

In conclusion, the application of the HODMD algorithm to the analysis of cardiac flows has not only the potential to deepen our insight into the intricate physics governing this complex phenomenon, but also may be of use as a valuable tool for identifying and foreseeing the temporal progression of CVDs. Through its ability to unravel the flow patterns within the LV, HODMD illuminates the path to more precise and targeted interventions.

4. Future directions

A recent study modelled the whole beating heart hemodynamics with the inclusion of valves and electrophysiology (Fedele et al., 2023). However, we are still far away from replicating the physiological phenomena. It is recommended to use the following advancements to move closer towards replication of *in vivo* flow and material properties.

4.1 Imaging and segmentation

Current limitations in temporal and spatial resolutions of imaging techniques restricts the acquisition of heart valve anatomies, myocardium thickness and structures, papillary muscles and *chordae tendineae*. The inclusion of these anatomical features in vortex analysis would give a more accurate and closer picture of *in vivo* flow patterns. The inclusion of papillary muscles may change the vortex patterns by obstructing the blood flow stream and vortices. Segmentation of such minute anatomic features is a major challenge. One possible avenue to overcome this obstruction would be developing neural network algorithms for segmentation. Machine learning-based algorithms could be explored then to interpolate these structures from available weak anatomical features.

4.2 Numerical simulation

The wall movement of the LV has been modelled so far by dynamic meshing features in each available study. However, the surface meshes used and their respective time instances during the cardiac cycle must match to accurately predict the flow patterns in the LV. Interpolation techniques are used for intermediate surface meshes during transient simulations. It is very difficult to interpolate the surface movement by including moving heart valves and papillary muscles. Also, patient-specific boundary conditions are needed for inlet velocity/pressure at local regions, and they can be measured using probes in each patient. The aortic and MV properties can be replicated using a heart muscle stress test, and this could be implemented into numerical simulations. The computational time and cost of cardiovascular simulations are decreasing rapidly, and it can be extended by parallelising the flow solvers. The cost of computer

https://doi.org/10.1017/flo.2025.6 Published online by Cambridge University Press

simulation per Gflop is less than a cent of a dollar, which can be utilised in patient care by including numerical simulations in medical practice.

4.3 Analysis of results using trained models

Cardiovascular simulations are time consuming due to human interventions at every step and the time required can be reduced by automating the numerical simulations from loading images to post-processing of results. The vortex patterns in LV can be analysed by machine learning-trained algorithms on various scales of healthy, moderate to severe diseases. After gaining large and rich CFD data on the vortex dynamics for a large population, it could be possible to train neural networks and obtain vortex parameters using just an anatomic model of the heart.

The inclusion of the above suggestions will significantly contribute to increasing the applicability of CFD simulations in daily clinical practice and pre-operative and post-operative surgery planning and evaluation. The use of increased computational capability and lower cost will enhance the inclusion of *in silico* medicine in clinical practice and decision making. The US Food and Drug Administration (FDA) recommends using computer simulations to complement human or animal testing. Recently, the FDA approved multiple computer programs that are useful in the treatment and management of CVDs (Ahmed et al., 2023; Morrison et al., 2018).

Funding statement. The authors acknowledge the grants TED2021-129774B-C21 and PLEC2022-009235 funded by MCIN/AEI/10.13039/501100011033 and by the European Union "NextGenerationEU"/PRTR and the grant PID2023-147790OB-I00 funded by MCIU/AEI/10.13039/501100011033/FEDER, UE. The authors gratefully acknowledge the Universidad Politécnica de Madrid (www.upm.es) for providing computing resources on the Magerit Supercomputer.

Competing interests. The authors declare that they have no known competing financial interests or personal relationships that could have appeared to influence the work reported in this paper.

Data availability statement. Not applicable.

References

Abe, H., Caracciolo, G., Kheradvar, A., Pedrizzetti, G., Khandheria, B. K., Narula, J., & Sengupta, P. P. (2013). Contrast echocardiography for assessing left ventricular vortex strength in heart failure: A prospective cohort study. *European Heart Journal Cardiovascular Imaging*, *14*(11), 1049–1060. https://doi.org/10.1093/ehjci/jet049

Adabifirouzjaei, F., Igata, S., Strachan, M., & DeMaria, A. N. (2021). Diastolic left ventricular energy loss: Relation to age, phase of diastole, and flow velocity. *Journal of the American Society of Echocardiography*, *34*(6), 698–700. https://doi.org/10.1016/j.echo.2021.02.011

Ahmed, K. B. R., Pathmanathan, P., Kabadi, SV., Drgon, T., & Morrison, T. M. (2023). *Editorial on the FDA report on "Successes and opportunities in modeling & simulation for FDA* (pp. 6–9. Annals of Biomedical Engineering. Springer, https://doi.org/10.1007/s10439-022-03112-x January 1

Al-Azawy, M. G., Turan, A., & Revell, A. (2017). Investigating the impact of non-Newtonian blood models within a heart pump. *International Journal for Numerical Methods in Biomedical Engineering*, *33*(1), e02780.

ANSYS, R. (2022). Fluent, Release 22.1, Help System, Theory Guide. Canonsburg, PA, USA: ANSYS. Inc.

Antiga, L., Piccinelli, M., Botti, L., Ene-Iordache, B., Remuzzi, A., & Steinman, D. A. (2008). An image-based modeling framework for patient-specific computational hemodynamics. *Medical and Biological Engineering and Computing*, *46*(11), 1097–1112. https://doi.org/10.1007/s11517-008-0420-1

Baccani, B., Domenichini, F., & Pedrizzetti, G. (2002a). Vortex dynamics in a model left ventricle during filling. *European Journal of Mechanics - B/Fluids*, *21*(5), 527–543.

Baccani, B., Domenichini, F., Pedrizzetti, G., & Tonti, G. (2002b). Fluid dynamics of the left ventricular filling in dilated cardiomyopathy. *Journal of Biomechanics*, *35*(5), 665–671. https://doi.org/10.1016/S0021-9290(02)00005-2

Becker, K. C., Cohen, J., Nyce, J. D., Yau, J. L., Uppu, S. C., Sangupta, P. P., & Srivastava, S. (2023). Age-related changes in left ventricular vortex and energy loss patterns: from newborns to adults. *American Journal of Physiology-Heart and Circulatory Physiology*, *324*(5), H624–H629. https://doi.org/10.1152/ajpheart.00002.2023 February).

Bell-Navas, A., Groun, N., Villalba-Orero, M., Lara-Pezzi, E., Garicano-Mena, J., & Le Clainche, S. (2025). Automatic cardiac pathology recognition in echocardiography images using higher order dynamic mode decomposition and a vision transformer for small datasets. *Expert Systems with Applications*, *264*, 125849.

Bennati, L., Vergara, C., Giambruno, V., Fumagalli, I., Corno, A. F., Quarteroni, A., Puppini, G., & Luciani, G. B. (2023). An image-based computational fluid dynamics study of mitral regurgitation in presence of prolapse. *Cardiovascular Engineering and Technology*, *14*(3), 457–475.

Berikol, G. B., Yildiz, O., & Özcan, T. (2016). Diagnosis of acute coronary syndrome with a support vector machine. *Journal of Medical Systems*, *40*(4), 1–8. https://doi.org/10.1007/s10916-016-0432-6

Berlot, B., Moya Mur, J. L., Jug, B., Rodríguez Muñoz, D., Megias, A., Casas Rojo, E., Fernández-Golfín, C., & Zamorano, J. L. (2019). Effect of diastolic dysfunction on intraventricular velocity behavior in early diastole by flow mapping. *International Journal of Cardiovascular Imaging*, *35*(9), 1627–1636. https://doi.org/10.1007/s10554-019-01612-x

Bermejo, J., Benito, Y., Alhama, M., Yotti, R., Martínez-Legazpi, P., del Villar, C. P., Pérez-David, E., González-Mansilla, A., Santa-Marta, C., Barrio, A., Fernández-Avilés, F., & del Álamo, J. C. (2014). Intraventricular vortex properties in non-ischemic dilated cardiomyopathy. *American Journal of Physiology-Heart and Circulatory Physiology*, *306*(5), 718–729. https://doi.org/10.1152/ajpheart.00697.2013

Brindise, M. C., Meyers, B. A., & Vlachos, P. P. (2020). Universality of vortex ring decay in the left ventricle. *Journal of Biomechanics*, *103*, 109695. https://doi.org/10.1016/j.jbiomech.2020.109695

Bucelli, M., Zingaro, A., Africa, P. C., Fumagalli, I., Dede', L., & Quarteroni, A. (2023). A mathematical model that integrates cardiac electrophysiology, mechanics, and fluid dynamics: Application to the human left heart. *International Journal for Numerical Methods in Biomedical Engineering*, *39*(3), 1–37. https://doi.org/10.1002/cnm.3678 2022-12.

Chan, B. T., Abu Osman, N. A., Lim, E., Chee, K. H., Abdul Aziz, Y. F., Abed, A. A., Lovell, N. H., Dokos, S., & Bauer, W. R. (2013a). Sensitivity Analysis of Left Ventricle with Dilated Cardiomyopathy in Fluid Structure Simulation. *PLoS ONE*, *8*(6), 1–11. https://doi.org/10.1371/journal.pone.0067097

Chan, B. T., Ahmad Bakir, A., Al Abed, A., Dokos, S., Leong, C. N., Ooi, E. H., Lim, R., & Lim, E. (2019). Impact of myocardial infarction on intraventricular vortex and flow energetics assessed using computational simulations. *International Journal for Numerical Methods in Biomedical Engineering*, *35*(6), 1–17. https://doi.org/10.1002/cnm.3204

Chan, B. T., Lim, E., Chee, K. H., & Abu Osman, N. A. (2013b). Review on CFD simulation in heart with dilated cardiomyopathy and myocardial infarction. *Computers in Biology and Medicine*, *43*(4), 377–385. https://doi.org/10.1016/j.compbiomed.2013.01.013

Chan, B. T., Lim, E., Ong, C. W., & Abu Osman, N. A. (2013c). Effect of spatial inlet velocity profiles on the vortex formation pattern in a dilated left ventricle. *Computer Methods in Biomechanics and Biomedical Engineering*, *18*(1), 90–96. https://doi.org/10.1080/10255842.2013.779683

Chan, B. T., Yeoh, H. K., Liew, Y. M., Aziz, Y. F. A., Sridhar, G. S., Hamilton-Craig, C., Platts, D., & Lim, E. (2017). Left ventricular flow propagation velocity measurement: Is it cast in stone? *Medical and Biological Engineering and Computing*, *55*(10), 1883–1893. https://doi.org/10.1007/s11517-017-1639-5

Cheng, Y., Oertel, H., & Schenkel, T. (2005). Fluid-structure coupled CFD simulation of the left ventricular flow during filling phase. *Annals of Biomedical Engineering*, *33*(5), 567–576. https://doi.org/10.1007/s10439-005-4388-9

Chnafa, C., Mendez, S., & Nicoud, F. (2014). Image-based large-eddy simulation in a realistic left heart. *Computers and Fluids*, *94*, 173–187. https://doi.org/10.1016/j.compfluid.2014.01.030

Cho, Y. I., & Kensey, K. R. (1991). Effects of the non-Newtonian viscosity of blood on flows in a diseased arterial vessel. Part 1: Steady flows. *Biorheology*, *28*(3-4), 241–262. https://doi.org/10.3233/BIR-1991-283-415

Collia, D., Libero, G., Pedrizzetti, G., & Ciriello, V. (2022). Surrogate models provide new insights on metrics based on blood flow for the assessment of left ventricular function. *Scientific Reports*, *12*(1), 8695. https://doi.org/10.1038/s41598-022-12560-3

Collia, D., Zovatto, L., Tonti, G., & Pedrizzetti, G. (2021). Comparative analysis of right ventricle fluid dynamics. *Frontiers in Bioengineering and Biotechnology*, *9*, 1–10. https://doi.org/10.3389/fbioe.2021.667408 July

Colorado-Cervantes, J. I., Nardinocchi, P., Piras, P., Sansalone, V., Teresi, L., Torromeo, C., & Puddu, P. E. (2022). Patient-specific modeling of left ventricle mechanics. *Acta Mechanica Sinica/Lixue Xuebao*, *38*(1). https://doi.org/10.1007/s10409-021-09041-0

COMSOL (2018). Multiphysics, C. O. M. S. O. L. 3.4. Stockholm, Sweden: COMSOL AB.

Dabiri, J. O. (2009). Optimal vortex formation as a unifying principle in biological propulsion. *Annual Review of Fluid Mechanics*, *41*(1), 17–33. https://doi.org/10.1146/annurev.fluid.010908.165232

Dabiri, J. O., & Gharib, M. (2004). Delay of vortex ring pinchoff by an imposed bulk counterflow. *Physics of Fluids*, *16*(4), L28–L30. https://doi.org/10.1063/1.1669353

Dahl, S. K., Thomassen, E., Hellevik, L. R., & Skallerud, B. (2012). Impact of pulmonary venous locations on the intra-atrial flow and the mitral valve plane velocity profile. *Cardiovascular Engineering and Technology*, *3*(3), 269–281. https://doi.org/10.1007/s13239-012-0099-1

De Vita, F., de Tullio, M. D., & Verzicco, R. (2016). Numerical simulation of the non-Newtonian blood flow through a mechanical aortic valve: Non-Newtonian blood flow in the aortic root. *Theoretical and Computational Fluid Dynamics*, *30*(1–2), 129–138. https://doi.org/10.1007/s00162-015-0369-2

Di Labbio, G., & Kadem, L. (2018). Jet collisions and vortex reversal in the human left ventricle. *Journal of Biomechanics*, *78*, 155–160. https://doi.org/10.1016/j.jbiomech.2018.07.023

Di Labbio, G., Thiffeault, J. L., & Kadem, L. (2022). Braids in the heart: Global measures of mixing for cardiovascular flows. *Flow*, *2*, E12. https://doi.org/10.1017/flo.2022.6

Doenst, T., Spiegel, K., Reik, M., Markl, M., Hennig, J., Nitzsche, S., Beyersdorf, F., & Oertel, H. (2009). Fluid-dynamic modeling of the human left ventricle: Methodology and application to surgical ventricular reconstruction. *Annals of Thoracic Surgery*, *87*(4), 1187–1195. https://doi.org/10.1016/j.athoracsur.2009.01.036

Domenichini, F., & Pedrizzetti, G. (2016). Hemodynamic forces in a model left ventricle. *Physical Review Fluids*, *1*(8), 083201. https://doi.org/10.1103/PhysRevFluids.1.083201

Domenichini, F., Pedrizzetti, G., & Baccani, B. (2005). Three-dimensional filling flow into a model left ventricle. *Journal of Fluid Mechanics*, *539*(-1), 179–198. https://doi.org/10.1017/S0022112005005550

Domenichini, F., Querzoli, G., Cenedese, A., & Pedrizzetti, G. (2007). Combined experimental and numerical analysis of the flow structure into the left ventricle. *Journal of Biomechanics*, *40*(9), 1988–1994. https://doi.org/10.1016/j.jbiomech.2006.09.024

Doost, S. N., Ghista, D., Su, B., Zhong, L., & Morsi, Y. S. (2016a). Heart blood flow simulation: A perspective review. *BioMedical Engineering Online*, *15*(1), 1–28. https://doi.org/10.1186/s12938-016-0224-8

Doost, S. N., Zhong, L., Su, B., & Morsi, Y. S. (2016b). The numerical analysis of non-Newtonian blood flow in human patient-specific left ventricle. *Computer Methods and Programs in Biomedicine*, *127*, 232–247. https://doi.org/10.1016/j.cmpb.2015.12.020

Elbaz, M. S., Calkoen, E. E., Westenberg, J. J., Lelieveldt, B. P., Roest, A. A., & Van Der Geest, R. J. (2014). Vortex flow during early and late left ventricular filling in normal subjects: Quantitative characterization using retrospectively-gated 4D flow cardiovascular magnetic resonance and three-dimensional vortex core analysis. *Journal of Cardiovascular Magnetic Resonance*, *16*(1), 78.

Eriksson, J., Bolger, A. F., Ebbers, T., & Carlhäll, C. J. (2013). Four-dimensional blood flow-specific markers of LV dysfunction in dilated cardiomyopathy. *European Heart Journal Cardiovascular Imaging*, *14*(5), 417–424. https://doi.org/10.1093/ehjci/jes159

Fathi, M. F., Bakhshinejad, A., Baghaie, A., Saloner, D., Sacho, R. H., Rayz, V. L., & D'Souza, R. M. (2018). Denoising and spatial resolution enhancement of 4D flow MRI using proper orthogonal decomposition and lasso regularization. *Computerized Medical Imaging and Graphics*, *70*, 165–172. https://doi.org/10.1016/j.compmedimag.2018.07.003

Fedele, M., Piersanti, R., Regazzoni, F., Salvador, M., Africa, P. C., Bucelli, M., Zingaro, A., Dede', L., & Quarteroni, A. (2023). A comprehensive and biophysically detailed computational model of the whole human heart electromechanics. *Computer Methods in Applied Mechanics and Engineering*, *410*, 115983. https://doi.org/10.1016/j.cma.2023.115983

Fedele, M., & Quarteroni, A. (2021). Polygonal surface processing and mesh generation tools for the numerical simulation of the cardiac function. *International Journal for Numerical Methods in Biomedical Engineering*, *37*(4), 1–34. https://doi.org/10.1002/cnm.3435

Fortini, S., Querzoli, G., Espa, S., & Cenedese, A. (2013). Three-dimensional structure of the flow inside the left ventricle of the human heart. *Experiments in Fluids*, *54*(11), 1–9. https://doi.org/10.1007/s00348-013-1609-0

Fu, J. F., Klyuzhin, I. S., McKeown, M. J., Stoessl, A. J., & Sossi, V. (2020). Novel data-driven, equation-free method captures spatio-temporal patterns of neurodegeneration in Parkinson's disease: Application of dynamic mode decomposition to PET. *NeuroImage: Clinical*, *25*, 102150. https://doi.org/10.1016/j.nicl.2019.102150

Gao, H., Feng, L., Qi, N., Berry, C., Griffith, B. E., & Luo, X. (2017). A coupled mitral valve—left ventricle model with fluid-structure interaction. *Medical Engineering and Physics*, *47*, 128–136. https://doi.org/10.1016/j.medengphy.2017.06.042

Gharib, M., Rambod, E., Kheradvar, A., Sahn, D. J., & Dabiri, J. O. (2006). Optimal vortex formation as an index of cardiac health. *Proceedings of National Academy of Sciences of United States of America*, *103*(16), 6305–6308. https://doi.org/10.1073/pnas.0600520103

Gharib, M., Rambod, E., & Shariff, K. (1998). A universal time scale for vortex ring formation. *Journal of Fluid Mechanics*, *360*, 121–140. https://doi.org/10.1017/S0022112097008410

Goubergrits, L., Vellguth, K., Obermeier, L., Schlief, A., Tautz, L., Bruening, J., Lamecker, H., Szengel, A., Nemchyna, O., Knosalla, C., Kuehne, T., & Solowjowa, N. (2022). CT-based analysis of left ventricular hemodynamics using statistical shape modeling and computational fluid dynamics. *Frontiers in Cardiovascular Medicine*, *9*, 901902. https://doi.org/10.3389/fcvm.2022.901902

Grinberg, L., Yakhot, A., & Karniadakis, G. E. (2009). Analyzing transient turbulence in a stenosed carotid artery by proper orthogonal decomposition. *Annals of Biomedical Engineering*, *37*(11), 2200–2217. https://doi.org/10.1007/s10439-009-9769-z

Grossman, W., McLaurin, L. P., Moos, S. P., Stefadouros, M., & Young, D. T. (1974). Wall thickness and diastolic properties of the left ventricle. *Circulation*, *49*(1), 129–135.

Groun, N., Villalba-Orero, M., Lara-Pezzi, E., Valero, E., Garicano-Mena, J., & Le Clainche, S. (2022). Higher order dynamic mode decomposition: From fluid dynamics to heart disease analysis. *Computers in Biology and Medicine*, *144*, 105384. https://doi.org/10.1016/j.compbiomed.2022.105384

Grünwald, A., Korte, J., Wilmanns, N., Winkler, C., Linden, K., Herberg, U., Groß-Hardt, S., Steinseifer, U., & Neidlin, M. (2022). Intraventricular flow simulations in singular right ventricles reveal deteriorated washout and low vortex formation. *Cardiovascular Engineering and Technology*, *13*(3), 495–503. https://doi.org/10.1007/s13239-021-00598-9

Gülan, U., Rossi, V. A., Gotschy, A., Saguner, A. M., Manka, R., Brunckhorst, C. B., Duru, F., Schmied, C. M., & Niederseer, D. (2022). A comparative study on the analysis of hemodynamics in the athlete's heart. *Scientific Reports*, *12*(1), 1–7. https://doi.org/10.1038/s41598-022-20839-8

Han, Y., Huang, L., Li, Z., Ma, N., Li, Q., Li, Y., Wu, L., Zhang, X., Wu, X., Che, X., & Zhang, H. (2019). Relationship between left ventricular isovolumic relaxation flow patterns and mitral inflow patterns studied by using vector flow mapping. *Scientific Reports*, *9*(1), 1–8. https://doi.org/10.1038/s41598-019-52680-x

Hara, H., Virmani, R., Holmes, D. R., Buchbinder, M., Lesser, J. R., van Tassel, R. A., Mooney, M. R., & Schwartz, R. S. (2009). Is the left atrial appendage more than a simple appendage? *Catheterization and Cardiovascular Interventions*, *74*(2), 234–242. https://doi.org/10.1002/ccd.21983

He, G., Han, L., Zhang, J., Shah, A., Kaczorowski, D. J., Griffith, B. P., & Wu, Z. (2022). Numerical study of the effect of LVAD inflow cannula positioning on thrombosis risk. *Computer Methods in Biomechanics and Biomedical Engineering*, *25*(8), 852–860. https://doi.org/10.1080/10255842.2021.1984433

Human Heart (2023). Image source: Wikimedia Commons. https://upload.wikimedia.org/wikipedia/commons/e/e5/Diagram_of_the_human_heart_%28cropped%29.svg

Henderson, A. (2007). *ParaView guide, a parallel visualization application, Kitware inc*. Kitware Inc.

Heppell, R. M., Berkin, K. E., McLenachan, J. M., & Davies, J. A. (1997). Haemostatic and haemodynamic abnormalities associated with left atrial thrombosis in non-rheumatic atrial fibrillation. *Heart*, *77*(5), 407–411. https://doi.org/10.1136/hrt.77.5.407

Hu, L. W., Xiang, Y., Qin, S. Y., Ouyang, R. Z., Liu, J. L., Peng, Y. F., Xie, W. H., Zhang, Y., Liu, H., & Zhong, Y. M. (2022). Vortex formation time as an index of left ventricular filling efficiency: Comparison between children volunteers and patients with tetralogy of fallot. *Translational Pediatrics*, *11*(6), 869–881. https://doi.org/10.21037/tp-22-67

Jefferies, J. L., & Towbin, J. A. (2010). Dilated cardiomyopathy. *The Lancet*, *375*(9716), 752–762. https://doi.org/10.1016/S0140-6736(09)62023-7

Khalafvand, S. S., Hung, T., Ng, E. Y., & Zhong, L. (2015). Kinematic, dynamic, and energy characteristics of diastolic flow in the left ventricle. *Computational and Mathematical Methods in Medicine*, *2015*, 1–12. https://doi.org/10.1155/2015/701945

Kheradvar, A., Assadi, R., Falahatpisheh, A., & Sengupta, P. P. (2012). Assessment of transmitral vortex formation in patients with diastolic dysfunction. *Journal of the American Society of Echocardiography*, *25*(2), 220–227. https://doi.org/10.1016/j.echo.2011.10.003

Kheradvar, A., & Gharib, M. (2007). Influence of ventricular pressure drop on mitral annulus dynamics through the process of vortex ring formation. *Annals of Biomedical Engineering*, *35*(12), 2050–2064. https://doi.org/10.1007/s10439-007-9382-y

Kheradvar, A., & Gharib, M. (2009). On mitral valve dynamics and its connection to early diastolic flow. *Annals of Biomedical Engineering*, *37*(1), 1–13. https://doi.org/10.1007/s10439-008-9588-7

Kheradvar, A., Houle, H., Pedrizzetti, G., Tonti, G., Belcik, T., Ashraf, M., Lindner, J. R., Gharib, M., & Sahn, D. (2010). Echocardiographic particle image velocimetry: A novel technique for quantification of left ventricular blood vorticity pattern. *Journal of the American Society of Echocardiography*, *23*(1), 86–94. https://doi.org/10.1016/j.echo.2009.09.007

Kilner, P. J., Yang, G. Z., Wilkest, A. J., Mohladdlin, R. H., Firmin, D. N., & Yacoub, M. H. (2000). Asymmetric redirection of flow through the heart. *Nature*, *404*(6779), 759–761. https://doi.org/10.1038/35008075

Kikinis, R., Pieper, S. D., & Vosburgh, K.G. (2013). 3D slicer: A platform for subject-specific image analysis, visualization, and clinical support. In *In intraoperative imaging and image-guided therapy* (pp. 277–289). New York, NY: Springer New York.

Klein, S., Staring, M., Murphy, K., Viergever, M. A., & Pluim, J. P. W. (2010). Elastix: A toolbox for intensity-based medical image registration. *IEEE Transactions on Medical Imaging*, *29*(1), 196–205. https://doi.org/10.1109/TMI.2009.2035616

Korte, J., Rauwolf, T., Thiel, J. N., Mitrasch, A., Groschopp, P., Neidlin, M., Schmeißer, A., Braun-Dullaeus, R., & Berg, P. (2023). Hemodynamic assessment of the pathological left ventricle function under rest and exercise conditions. *Fluids*, *8*(2), 1–15. https://doi.org/10.3390/fluids8020071

Krueger, P. S., & Gharib, M. (2003). The significance of vortex ring formation to the impulse and thrust of a starting jet. *Physics of Fluids*, *15*(5), 1271–1281. https://doi.org/10.1063/1.1564600

Ku, D. N. (1997). Blood flow in arteries. *Annual Review of Fluid Mechanics*, *29*(1), 399–434. https://doi.org/10.1146/annurev.fluid.29.1.399

La Gerche, A., Pedrizzetti, G., Ranieri, B., D.'Andrea, A., & Bossone, E. (2022). On the characterization of athlete's heart using 3D echocardiography. *European Journal of Preventive Cardiology*, *29*(12), 1592–1593. https://doi.org/10.1093/eurjpc/zwac117

Lantz, J., Gupta, V., Henriksson, L., Karlsson, M., Persson, A., Carlhäll, C. J., & Ebbers, T. (2019). Impact of pulmonary venous inflow on cardiac flow simulations: Comparison with In Vivo 4D flow MRI. *Annals of Biomedical Engineering*, *47*(2), 413–424. https://doi.org/10.1007/s10439-018-02153-5

Liao, S., Simpson, B., Neidlin, M., Kaufmann, T. A. S., Li, Z., Woodruff, M. A., & Gregory, S. D. (2016). Numerical prediction of thrombus risk in an anatomically dilated left ventricle: The effect of inflow cannula designs. *BioMedical Engineering Online*, *15*(s2), 587–604. https://doi.org/10.1186/s12938-016-0262-2

Loerakker, S., Cox, L. G. E., van Heijst, G. J. F., de Mol, B. A. J. M., & van de Vosse, F. N. (2008). Influence of dilated cardiomyopathy and a left ventricular assist device on vortex dynamics in the left ventricle. *Computer Methods in Biomechanics and Biomedical Engineering*, *11*(6), 649–660. https://doi.org/10.1080/10255840802469379

Mangual, J. O., Kraigher-krainer, E., De, Luca A., Toncelli, L., Shah, A., Solomon, S., Galanti, G., Domenichini, F., & Pedrizzetti, G. (2013). Comparative numerical study on left ventricular fluid dynamics after dilated cardiomyopathy. *Journal of Biomechanics*, *46*(10), 1611–1617. https://doi.org/10.1016/j.jbiomech.2013.04.012

Mao, W., Caballero, A., McKay, R., Primiano, C., & Sun, W. (2017). Fully-coupled fluid-structure interaction simulation of the aortic and mitral valves in a realistic 3D left ventricle model. *PLoS ONE*, *12*(9), 1–21. https://doi.org/10.1371/journal.pone.0184729

Martínez-Legazpi, P., Bermejo, J., Benito, Y., Yotti, R., Pérez del Villar, C., González-Mansilla, A., Barrio, A., Villacorta, E., Sánchez, P. L., Fernández-Avilés, F., & del Álamo, J. C. (2014). Contribution of the diastolic vortex ring to left ventricular filling. *Journal of the American College of Cardiology*, *64*(16), 1711–1721.

Matsuura, K., Shiraishi, K., Sato, K., Shimada, K., Goya, S., Uemura, A., Ifuku, M., Iso, T., Takahashi, K., & Tanaka, R. (2019). Left ventricular vortex and intraventricular pressure difference in dogs under various loading conditions. *American Journal of Physiology - Heart and Circulatory Physiology*, *316*(4), H882–H888. https://doi.org/10.1152/ajpheart.00686.2018

Mele, D., Smarrazzo, V., Pedrizzetti, G., Capasso, F., Pepe, M., Severino, S., Luisi, G. A., Maglione, M., & Ferrari, R. (2018). Intracardiac flow analysis : Techniques and potential clinical applications. *Journal of the American Society of Echocardiography*, *32*(3), 319–332. https://doi.org/10.1016/j.echo.2018.10.018

Meschini, V., De Tullio, M. D., Querzoli, G., & Verzicco, R. (2018). Flow structure in healthy and pathological left ventricles with natural and prosthetic mitral valves. *Journal of Fluid Mechanics*, *834*, 271–307. https://doi.org/10.1017/jfm.2017.725

Meschini, V., Mittal, R., & Verzicco, R. (2021). Systolic anterior motion in hypertrophic cardiomyopathy : A fluid – structure interaction computational model. *Theoretical and Computational Fluid Dynamics*, *35*(3), 381–396. https://doi.org/10.1007/s00162-021-00564-0

Mitchell, S. C., Bosch, J. G., Lelieveldt, B. P. F., Van der Geest, R. J., Reiber, JHC., & Sonka, M. (2002). 3-D active appearance models: Segmentation of cardiac MR and ultrasound images. *IEEE Transactions on Medical Imaging*, *21*(9), 1167–1178. https://doi.org/10.1109/TMI.2002.804425

Monosilio, S., Filomena, D., Sannino, M., Birtolo, I., Cimino, S., Tonti, G., Pedrizzetti, G., Benedetti, G., Fedele, F., Maestrini, V., & Agati, L. (2022). Left ventricular forces distribution in patients with heart failure and reduced ejection fraction. *European Heart Journal - Cardiovascular Imaging*, *23*(Supplement_1), 247–248. https://doi.org/10.1093/ehjci/jeab289.179

Morrison, T. M., Pathmanathan, P., Adwan, M., & Margerrison, E. (2018). Advancing regulatory science with computational modeling for medical devices at the FDA's office of science and engineering laboratories. *Frontiers in Medicine*, *5*, 241. https://doi.org/10.3389/fmed.2018.00241

Njoku, P., Wardley, J., & Garg, P. (2022). Streamline–based three–dimensional peak–velocity tracing of transvalvular flow using four - dimensional flow cardiac magnetic resonance imaging for left ventricular diastolic assessment in aortic regurgitation : A case report. *Journal of Medical Case Reports*, *16*(1), 1–5. https://doi.org/10.1186/s13256-022-03422-7

Obermeier, L., Vellguth, K., Schlief, A., Tautz, L., Bruening, J., Knosalla, C., Kuehne, T., Solowjowa, N., & Goubergrits, L. (2022). CT-based simulation of left ventricular hemodynamics: A pilot study in mitral regurgitation and left ventricle aneurysm patients. *Frontiers in Cardiovascular Medicine*, *9*, 828556. https://doi.org/10.3389/fcvm.2022.828556

Pasipoularides, A., Vlachos, P. P., & Little, W. C. (2015). Vortex formation time is not an index of ventricular function. *Advances in Data Analysis and Classification*, *9*(1), 54–58. https://doi.org/10.1007/s12265-015-9607-7

Pedrizzetti, G., & Domenichini, F. (2005). Nature optimizes the swirling flow in the human left ventricle. *Physical Review Letters*, *95*(10), 1–4. https://doi.org/10.1103/PhysRevLett.95.108101

Pedrizzetti, G., & Domenichini, F. (2015). Left ventricular fluid mechanics: The long way from theoretical models to clinical applications. *Annals of Biomedical Engineering*, *43*(1), 26–40. https://doi.org/10.1007/s10439-014-1101-x

Pedrizzetti, G., La, Canna G., Alfieri, O., & Tonti, G. (2014). *The vortex—an early predictor of cardiovascular outcome?*. Nature Publishing Group, https://doi.org/10.1038/nrcardio.2014.75

Pedrizzetti, G., & Sengupta, P. P. (2015). Vortex imaging: New information gain from tracking cardiac energy loss. *European Heart Journal Cardiovascular Imaging*, *16*(7), 719–720. https://doi.org/10.1093/ehjci/jev070

Peng, P., Lekadir, K., Gooya, A., Shao, L., Petersen, S. E., & Frangi, A. F. (2016). A review of heart chamber segmentation for structural and functional analysis using cardiac magnetic resonance imaging. *Magnetic Resonance Materials in Physics, Biology and Medicine*, *29*(2), 155–195. https://doi.org/10.1007/s10334-015-0521-4

Pierrakos, O., & Vlachos, P. P. (2006). The effect of vortex formation on left ventricular filling and mitral valve efficiency. *Journal of Biomechanical Engineering*, *128*(4), 527–539. https://doi.org/10.1115/1.2205863

Poh, K. K., Lee, L. C., Shen, L., Chong, E., Tan, Y. L., Chai, P., Yeo, T. C., & Wood, M. J. (2012). Left ventricular fluid dynamics in heart failure: Echocardiographic measurement and utilities of vortex formation time. *European Heart Journal - Cardiovascular Imaging*, *13*(5), 385–393. https://doi.org/10.1093/ejechocard/jer288

Renzi, F., Vargara, C., Fedele, M., Giambruno, V., Quarteroni, A. M., Puppini, G., & Luciani, G. B. (2023). Accurate and efficient 3D reconstruction of right heart shape and motion from multi-series cine-MRI. *bioRxiv*, 2023-06.

Saber, N. R., Wood, N. B., Gosman, A. D., Merrifield, R. D., Yang, G. Z., Charrier, C. L., Gatehouse, P. D., & Firmin, D. N. (2003). Progress towards patient-specific computational flow modeling of the left heart via combination of magnetic resonance imaging with computational fluid dynamics. *Annals of Biomedical Engineering*, *31*(1), 42–52. https://doi.org/10.1114/1.1533073

Saeed, M., Van, T. A., Krug, R., Hetts, S. W., & Wilson, M. W. (2015). Cardiac MR imaging: Current status and future direction. *Cardiovasc Diagnosis and Therapy*, *5*(4), 290–310. https://doi.org/10.3978/j.issn.2223-3652.2015.06.07

Schenkel, T., Malve, M., Reik, M., Markl, M., Jung, B., & Oertel, H. (2009). MRI-based CFD analysis of flow in a human left ventricle: Methodology and application to a healthy heart. *Annals of Biomedical Engineering*, *37*(3), 503–515. https://doi.org/10.1007/s10439-008-9627-4

Seo, J. H., Vedula, V., Abraham, T., Lardo, A. C., Dawoud, F., Luo, H., & Mittal, R. (2014). Effect of the mitral valve on diastolic flow patterns. *Physics of Fluids*, *26*(12), 121901. https://doi.org/10.1063/1.4904094

Song, Z., & Borazjani, I. (2015). The role of shape and heart rate on the performance of the left ventricle. *Journal of Biomechanical Engineering*, *137*(11), 1–6. https://doi.org/10.1115/1.4031468

Stewart, K. C., Charonko, J. C., Niebel, C. L., Little, W. C., & Vlachos, P. P. (2012). Left ventricular vortex formation is unaffected by diastolic impairment. *American journal of physiology. Heart and circulatory physiology*, *303*(10), 1255–1262. https://doi.org/10.1152/ajpheart.00093.2012.-Nor

Stugaard, M., Koriyama, H., Katsuki, K., Masuda, K., Asanuma, T., Takeda, Y., Sakata, Y., Itatani, K., & Nakatani, S. (2015). Energy loss in the left ventricle obtained by vector flow mapping as a new quantitative measure of severity of aortic regurgitation: A combined experimental and clinical study. *European Heart Journal - Cardiovascular Imaging*, *16*(7), 723–730. https://doi.org/10.1093/ehjci/jev035

Su, B., Tan, R. S., Tan, J. L., Guo, K. W. Q., Zhang, J. M., Leng, S., Zhao, X., Allen, J. C., & Zhong, L. (2016). Cardiac MRI based numerical modeling of left ventricular fluid dynamics with mitral valve incorporated. *Journal of Biomechanics*, *49*(7), 1199–1205. https://doi.org/10.1016/j.jbiomech.2016.03.008

Su, B., Zhong, L., Wang, X. K., Zhang, J. M., Tan, R. S., Allen, J. C., Tan, S. K., Kim, S., & Leo, H. L. (2014). Numerical simulation of patient-specific left ventricular model with both mitral and aortic valves by FSI approach. *Computer Methods and Programs in Biomedicine*, *113*(2), 474–482. https://doi.org/10.1016/j.cmpb.2013.11.009

Tagliabue, A., Dedè, L., & Quarteroni, A. (2017a). Complex blood flow patterns in an idealized left ventricle: A numerical study. *Chaos*, *27*(9), 093939. https://doi.org/10.1063/1.5002120

Tagliabue, A., Dedè, L., & Quarteroni, A. (2017b). Fluid dynamics of an idealized left ventricle: The extended Nitsche's method for the treatment of heart valves as mixed time varying boundary conditions. *International Journal for Numerical Methods in Fluids*, *85*(3), 135–164. https://doi.org/10.1002/fld.4375

Töger, J., Kanski, M., Carlsson, M., Kovács, S. J., Söderlind, G., Arheden, H., & Heiberg, E. (2012). Vortex ring formation in the left ventricle of the heart: Analysis by 4D flow MRI and Lagrangian coherent structures. *Annals of Biomedical Engineering*, *40*(12), 2652–2662. https://doi.org/10.1007/s10439-012-0615-3

van Assen, H. C., Danilouchkine, M. G., Frangi, A. F., Ordás, Sán, Westenberg, J. J. M., Reiber, J. H. C., & Lelieveldt, B. P. F. (2006). SPASM: A 3D-ASM for segmentation of sparse and arbitrarily oriented cardiac MRI data. *Medical Image Analysis*, *10*(2), 286–303. https://doi.org/10.1016/j.media.2005.12.001

Vedula, V., Fortini, S., Seo, J. H., Querzoli, G., & Mittal, R. (2014). Computational modeling and validation of intraventricular flow in a simple model of the left ventricle. *Theoretical and Computational Fluid Dynamics*, *28*(6), 589–604. https://doi.org/10.1007/s00162-014-0335-4

Vedula, V., George, R., Younes, L., & Mittal, R. (2015). Hemodynamics in the left atrium and its effect on ventricular flow patterns. *Journal of Biomechanical Engineering*, *137*(11), 1–8. https://doi.org/10.1115/1.4031487

Vierendeels, J. A., Riemslagh, K., Dick, E., & Verdonck, P. R. (2000). Computer simulation of intraventricular flow and pressure gradients during diastole. *Journal of Biomechanical Engineering*, *122*(6), 667–674.

Viola, F., Meschini, V., & Verzicco, R. (2020). Fluid–Structure-Electrophysiology interaction (FSEI) in the left-heart: A multi-way coupled computational model. *European Journal of Mechanics, B/Fluids*, *79*, 212–232.

Wei, Z. A., Huddleston, C., Trusty, P. M., Singh-Gryzbon, S., Fogel, M. A., Veneziani, A., & Yoganathan, A. P. (2019). Analysis of inlet velocity profiles in numerical assessment of Fontan hemodynamics. *Annals of Biomedical Engineering*, *47*(11), 2258–2270. https://doi.org/10.1007/s10439-019-02307-z

Wiener, P. C., Darwish, A., Friend, E., Kadem, L., & Pressman, G. S. (2021). Energy loss associated with In-vitro modeling of mitral annular calcification. *PLoS ONE*, *16*(2), e0246701. https://doi.org/10.1371/journal.pone.0246701

Worden, N. E., Lindower, P. D., Burns, T. L., Chatterjee, K., & Weiss, R. M. (2015). A second look with prone SPECT myocardial perfusion imaging reduces the need for angiography in patients at low risk for cardiac death or MI. *Journal of Nuclear Cardiology*, *22*(1), 115–122. https://doi.org/10.1007/s12350-014-9934-0

Xi, J., & Zhao, W. (2019). Correlating exhaled aerosol images to small airway obstructive diseases: A study with dynamic mode decomposition and machine learning. *PLoS ONE*, *14*(1), e0211413. https://doi.org/10.1371/journal.pone.0211413

Xiang, Y., Qin, S., & Liu, H. (2018). Patterns for efficient propulsion during the energy evolution of vortex rings. *European Journal of Mechanics - B/Fluids*, *71*, 47–58. https://doi.org/10.1016/j.euromechflu.2018.03.014

Yang, K., Wu, S., Zhang, H., Ghista, D. N., Samuel, O. W., & Wong, K. K. L. (2021). Lagrangian-averaged vorticity deviation of spiraling blood flow in the heart during isovolumic contraction and ejection phases. *Medical and Biological Engineering and Computing*, *59*(7–8), 1417–1430. https://doi.org/10.1007/s11517-021-02366-2

Zhang, A., Pan, M., Meng, L., Zhang, F., Zhou, W., Zhang, Y., & Zheng, R. (2021). Ultrasonic biomechanics method for vortex and wall motion of left ventricle : A phantom and in vivo study. *BMC Cardiovascular Disorders*, *21*(1), 1–10. https://doi.org/10.1186/s12872-021-02317-7

Zheng, X., Seo, J. H., Vedula, V., Abraham, T., & Mittal, R. (2012). Computational modeling and analysis of intracardiac flows in simple models of the left ventricle. *European Journal of Mechanics, B/Fluids*, *35*, 31–39. https://doi.org/10.1016/j.euromechflu.2012.03.002

Cite this article: Nagargoje M. S., Lazpita E., Garicano-Mena J. and Le Clainche S. (2025). A review on vortex dynamics in the healthy and dilated left ventricles and its application to heart health. *Flow*, *5*, E10. https://doi.org/10.1017/flo.2025.6